AD_____

AWARD NUMBER DAMD17-97-1-7325

TITLE: Development of Guidelines for the Prophylactic Treatment of Metastatically Involved Vertebral Bodies

PRINCIPAL INVESTIGATOR: Cari M. Whyne
Serena Hu, M.D.

CONTRACTING ORGANIZATION: University of California, San Francisco
San Francisco, California 94143-0962

REPORT DATE: August 1999

TYPE OF REPORT: Final

PREPARED FOR: U.S. Army Medical Research and Materiel Command
Fort Detrick, Maryland 21702-5012

REPORT DOCUMENTATION PAGE

Form Approved
OMB No. 0704-0188

1. AGENCY USE ONLY *(Leave blank)*	2. REPORT DATE	3. REPORT TYPE AND DATES COVERED
	August 1999	Final (15 Jul 97 – 14 Jul 99)

4. TITLE AND SUBTITLE
Development of Guidelines for the Prophylactic Treatment of Metastatically Involved Vertebral Bodies

5. FUNDING NUMBERS
DAMD17-97-1-7325

6. AUTHOR(S)
Cari M. Whyne

7. PERFORMING ORGANIZATION NAME(S) AND ADDRESS(ES)
University of California, San Francisco
San Francisco, California 94143-0962

8. PERFORMING ORGANIZATION REPORT NUMBER

9. SPONSORING / MONITORING AGENCY NAME(S) AND ADDRESS(ES)
U.S. Army Medical Research and Materiel Command
Fort Detrick, Maryland 21702-5012

10. SPONSORING / MONITORING AGENCY REPORT NUMBER

11. SUPPLEMENTARY NOTES

12a. DISTRIBUTION / AVAILABILITY STATEMENT
Approved for public release; distribution unlimited

12b. DISTRIBUTION CODE

13. ABSTRACT *(Maximum 200 words)*

Up to 1/3 of all cancer patients develop metastases to the spinal column and over 50% of spinal metastases with neurologic manifestations in females are found to arise from primary breast neoplasms (2). Using a combination of finite element modeling, materials and mechanical testing we aimed to quantify fracture risk in metastatically involved vertebral bodies in order to both understand the mechanism of burst fracture and develop a definitive set of clinical guidelines for the prophylactic treatment vertebral body metastases. To this end, we have determined the biphasic material properties of tumor tissue which has metastasized to bone and correlated these properties to tumor cellularity. We have demonstrated the importance of utilizing poroelasticity in modeling metastatically involved vertebral bodies. We constructed and experimentally validated a three-dimensional poroelastic finite element model of a metastatically involved spinal motion segment and parametrically assessed the effects of loading rate, tumor size, bone density and pedicle involvement on the risk of burst fracture and neurologic compromise. We have determined that the mechanism of burst fracture in the metastatically involved spine is due to pressurization of the vertebral body and elevated tensile hoop strains, causing failure of the posterior vertebral body wall.

14. SUBJECT TERMS	15. NUMBER OF PAGES
Breast Cancer, Vertebral Metastases, Burst Fracture, Biomechanics, Finite Element Modeling	28
	16. PRICE CODE

17. SECURITY CLASSIFICATION OF REPORT	18. SECURITY CLASSIFICATION OF THIS PAGE	19. SECURITY CLASSIFICATION OF ABSTRACT	20. LIMITATION OF ABSTRACT
Unclassified	Unclassified	Unclassified	Unlimited

FOREWORD

Opinions, interpretations, conclusions and recommendations are those of the author and are not necessarily endorsed by the U.S. Army.

____ Where copyrighted material is quoted, permission has been obtained to use such material.

____ Where material from documents designated for limited distribution is quoted, permission has been obtained to use the material.

____ Citations of commercial organizations and trade names in this report do not constitute an official Department of Army endorsement or approval of the products or services of these organizations.

____ In conducting research using animals, the investigator(s) adhered to the "Guide for the Care and Use of Laboratory Animals," prepared by the Committee on Care and use of Laboratory Animals of the Institute of Laboratory Resources, national Research Council (NIH Publication No. 86-23, Revised 1985).

/CW For the protection of human subjects, the investigator(s) adhered to policies of applicable Federal Law 45 CFR 46.

____ In conducting research utilizing recombinant DNA technology, the investigator(s) adhered to current guidelines promulgated by the National Institutes of Health.

____ In the conduct of research utilizing recombinant DNA, the investigator(s) adhered to the NIH Guidelines for Research Involving Recombinant DNA Molecules.

____ In the conduct of research involving hazardous organisms, the investigator(s) adhered to the CDC-NIH Guide for Biosafety in Microbiological and Biomedical Laboratories.

Lowell Thye Aug 10, 99

PI - Signature Date

TABLE OF CONTENTS

INTRODUCTION:

Breast, prostate, lung and renal cancers are the most common primary tumors which metastasize to bone. The vertebral column is the most frequent skeletal site for metastases (6) and due to the proximity to the spinal cord, 5% to 10% of all cancer patients develop neurologic manifestations (2). Up to 1/3 of all cancer patients develop metastases to the spinal column and over 50% of spinal metastases with neurologic manifestations in females are found to arise from primary breast neoplasms (2). In the face of greater life expectancy for women with breast cancer, spinal metastases are an increasing source of morbidity which negatively affects patients' long-term quality of life. Burst fracture is one of the most difficult injuries of the spine to successfully treat, in part because the exact mechanism by which the distraction forces are transmitted to the intracanal fragments of the burst fracture have not been adequately investigated (3). Fracture risk prediction has significant clinical importance, as prevention of fracture in high-risk patients may be possible through medical prophylaxis, use of external bracing, or internal stabilization. While improved imaging modalities allow clinicians to better determine the extent of bony metastases, assessing the risk of neurologic compromise is guesswork at best. A better understanding of spinal canal risk may permit some patients to avoid surgery altogether, an important goal in patients with limited life expectancy. Guidelines are needed to permit clinicians to select appropriate patients for intervention before the development of neurologic compromise. The purpose of our research is to quantify fracture risk in vertebral bodies affected by metastatic breast cancer in order to develop a set of clinical guidelines for the prophylactic treatment of patients with such metastases. We hypothesize that the use of poroelastic theory in modeling will yield more realistic estimates of fracture prediction compared to values based on a linear elastic model and that poroelastic properties of both bone and tumor tissue are necessary to understand the mechanisms of vertebral body failure and adequately assess the risk of neurologic compromise. The ultimate goal of this research is to use engineering analysis to develop clinical diagnostic and surgical guidelines for prophylactic stabilization of metastatically involved vertebral bodies in order to prevent paralysis and significantly improve the quality of life of patients with vertebral body metastases. The following is a summary of our progress towards those goals.

BODY:

Technical Objective 1: Poroelastic properties of breast tumor tissue
Task 1: To determine the poroelastic properties of tumor tissue which has metastasized to bone.

Lytic tumor tissue specimens were taken from human bone and tested under a confined compression uniaxial creep protocol. Specimens from 14 lytic tumors which had metastasized to bone were harvested. These include specimens from breast (29%), lung (21%), multiple myeloma (14%) and other cancers. Multiple specimens were tested for each tumor (with 3 exceptions due to small tumor size) to determine the intra-specimen variability due to both the testing protocol and inhomogeneities within the tumor. This resulted in a total of 27 specimens which underwent mechanical testing.

The mechanical behaviour of the tumor tissue was modeled using linear biphasic theory. The outcome variables for each specimen were the aggregate compressive modulus (H_A) and the hydraulic permeability (k). To determine these linear biphasic material properties of the tumor tissue specimens, the displacement vs time data was curve fit using a numerical minimization of least squares technique to the solution for creep displacement. Applied loads were adjusted so as to meet the small strain behaviour assumed in this theory.

Following testing, the histology of each tumor specimen was analyzed in conjunction with an adjacent piece of untested tissue. The specimens were immersed in formalin and run through an H & E stain. Visual inspection of the slides was used to determine the cellular vs. stromal content of the tissue present in each specimen. The cellularity data was organized into four groups: 0-25% cells, 25-50% cells, 50-75% cells, and 75-100% cells. Standard analysis of variance procedures were performed to compare specimen group means and to estimate the effect of the specimen variables (tumor type and cellularity) on the measured parameters of interest (H_A and k). A Fischer LSP test was used to determine differences between groups where appropriate.

The aggregate modulus (H_A) of the tumor tissue tested yielded a mean of 0.0034 MPa with a standard deviation of 0.0016 MPa. The mean hydraulic permeability (k) of the specimens was 0.61 mm^4/Ns with a standard deviation of 0.44 mm^4/Ns. The aggregate modulus of specimens with less than 50% cellularity was 76 percent higher than the aggregate modulus of more cellular tumors (0.0051 MPa vs 0.0029 MPa, $p<0.05$). As well, tumors with lower cellularity were found to have higher hydraulic permeabilities, although this result did not reach the level of statistical significance (<25% cellularity, k=1.13 mm^4/Ns; >25% cellularity, k=0.54 mm^4/Ns, p=0.066). No significant differences in aggregate modulus or hydraulic permeability were found between tumors of different types.

Tumor tissue specimens with a higher stromal content were found to behave stiffer than more cellular specimens ($p<0.05$). A higher percentage of stromal matrix increases the interconnectivity of the tumor tissue yielding both a higher compressive aggregate modulus and lower hydraulic permeability than more cellular specimens. No significant differences in mechanical properties were found between different tumor types. This finding is not surprising considering the histologic variation seen between tumors of the same type and even within different areas of individual specimens.

The values of H_A and k reported here are consistent with those measured for other hydrated tissues. For comparison, results from experimentation done on annulus fibrosus and cartilage have yielded much stiffer and less permeable results (annulus: H_A=0.12 MPa, k=0.013 mm^4/Ns; cartilage: H_A=0.3 to 1.5 MPa, k=0.01to 0.001 mm^4/Ns). The high fluid content of the tumors and the poor interconnectivity of the solid matrix would support the low aggregate modulus and high permeability values measured for this tissue.

Determination of tumor tissue material properties will enable the development of more accurate models of the metastatically involved spine which may be better able to simulate the pattern of burst fracture and clarify the risk of neurologic compromise. In addition, determination of the biphasic material properties of lytic lesions also has importance in developing effective tumor-drug transport models. In order for therapeutic agents to reach cancer cells, these large macromolecules must travel from the vessels across the interstitial matrix of the tumor. Higher permeabilities found in more cellular tumors may facilitate the transport of therapeutic agents to these metastases in comparison to tumors with higher stromal contents. Heterogeneous neoplasms, which incorporate areas of high cellularity and regions consisting mainly of stromal matrix may require sophisticated modeling to accurately gauge drug delivery throughout the tumor.

Technical Objective 2: Poroelastic theory applied to metastatically involved vertebral body modeling
Task 2: To develop a poroelastic two-dimensional axis-symmetric finite element model of the vertebral body and parametrically assess the effects of rate dependence on vertebral body strength and the implications of poroelastic theory in the consideration of metastatic involvement in the model.

We developed a two-dimensional axisymmetric finite element model of a spinal motion segment consisting of the first lumbar vertebral body and adjacent intervertebral disc (Figure 1). A finite element mesh consisting of 493 elements was generated and analyzed using commercial software (PATRAN 5.0, ABAQUS 5.6). The model was constructed to allow the inclusion of a centrally located tumor in the vertebral body, representing a 25% or 50% defect of the trabecular bone by volume. The intact model (no tumor included) was analyzed under a fully elastic configuration (both disc and vertebral body represented with elastic material properties), with a poroelastic disc attached to a linear elastic vertebral body (with and without restricted flow through the cartilaginous endplate), and as a fully poroelastic model. In the analyses of the metastatically involved cases only poroelastic modeling was performed.

The model was loaded axially under a uniform pressure of 1 MPa applied though the midplane of the intervertebral disc (which corresponds to a 1200N force, the compressive force on the lumbar spine for an individual standing upright holding an 8.3 kg mass with outstretched arms (21)). The intact poroelastic model was analyzed under a range of loading rates from 10,000 MPa/s (impact) to 4 MPa/s (slow walking). In the mixed elastic/poroelastic runs a physiologic loading rate level of 100MPa/s was applied. In the analyses of the metastatically involved cases poroelastic modeling was performed under loading rates of 10 MPa/s and 100MPa/s. We focused on trabecular bone failure and our outcome variables were: radial displacement of the vertebral body midline as an indicator for spinal canal encroachment, endplate deformation as a measure of endplate fracture, maximum strain indicating potential trabecular bone failure, and pore pressure to determine the amount of load carried by the fluid phase in the poroelastic analyses.

In assessing the need for utilizing poroelastic modeling techniques in analyzing spinal motion segments, it was found that the boundary conditions applied to the vertebral body endplate are dependent on the constitutive assumptions of the intervertebral disc, and as such, affect the strain and displacement results in the trabecular bone centrum. Greater disc deformation in the axial and radial directions in the fully elastic model create different loading conditions applied to the cortical endplate of the vertebral body, and thus different responses within the vertebral body itself. For analyses aimed at studying the responses of the intervertebral disc alone, our results suggest it is reasonable to utilize a mixed model. However, results for strains and displacements in the poroelastic vertebral body are not bounded by the mixed model results. The inclusion of the fluid phase into the vertebral body results in a portion of the spinal load being supported by the liquid, reducing the solid strains in the axial direction in the trabecular bone. Concurrently, the incompressibility of the fluid phase causes expansion and higher strains to develop in the radial direction within the vertebral body.

In examining the relative effects of tumor size, material properties and loading rate in the assessment of metastatically involved vertebral bodies, increased tumor size was found to cause the greatest increase in vertebral body displacements, strains and pore pressure. The location of maximum displacement and pore pressures suggest a greater risk for endplate and radial vertebral body failure (ie. an increased likelihood of vertebral burst fracture) as the size of defect increases. Greater maximum radial displacement values and increased tensile hoop strains predicted at the transverse midline of the vertebral body may potentially correspond to a catastrophic fracture pattern with bone and tumor encroachment into the spinal canal in a three-dimensional model. Loading rate was found to have the second strongest effect on metastatically involved vertebral body behavior. With inclusion of the poroelastic defect, increased loading rate resulted in more load carried by the fluid phase within the centrum, accounting for the increased pore pressures and lower axial compressive strains and displacements in the trabecular bone. Radial displacement along the transverse midline increased at higher loading rates, indicating escalating risk of potential neurologic compromise. These findings may indicate that the mechanism of burst fracture may differ in intact versus metastatically involved vertebral bodies. The presence of a defect which produces increased vertebral body pressurization and radial displacement may potentially allow a burst fracture pattern to occur without an endplate fracture. Variation of tumor tissue material properties did not have a large effect on the behavior of the trabecular bone centrum of the vertebral body, thus the primary site of the lytic tumor may not be of major significance in assessing failure risk. Results of this simplified analysis provide a justification for the use of more complex three-dimensional poroelastic models and demonstrate the importance of tumor size and loading rate.

Task 3: To incorporate poroelasticity and metastatic defects into the three-dimensional vertebral body model developed in the preliminary study.

We developed a three dimensional poroelastic finite element model of the first lumbar vertebra and adjacent intervertebral discs, symmetric about the sagittal plane and incorporating anatomical vertebral body curvature based on average values reported for L1 (1) (Figure 2a). The posterior arch was included in the model, although no other posterior elements were modeled. The model was designed to include a centrally located hemi-elliptical tumor occupying 15%, 30% or 45% of the trabecular bone centrum by volume. The mesh consisted of 5668 elements (20-noded bricks) and was generated and analyzed using commercial software (PATRAN 7.0; ABAQUS 5.7). The model was loaded in axial compression through the midplane of the superior intervertebral disc. Pressure loading boundary conditions were applied accompanied by multi point constraints to maintain the planarity of the superior disc midplane. The model was focused to examine both the mechanism of failure in the metastatically involved spine and the potential for neurologic deficit.

Technical Objective 3: Parametric analysis of burst fracture risk

Task 4: Apply a parametric analysis in the three-dimensional model to determine the sensitivity to the risk of posterior vertebral body fracture and neurologic compromise of the varied configurations.

In analyzing our model we focused on the variation of six parameters: tumor size, applied load, trabecular bone apparent density, loading rate, disc quality and pedicle involvement. In examining our results, we concentrated on the behaviour of the trabecular bone centrum and cortical shell of the vertebral body. As such, our outcome variables were: pore pressure generated in the vertebral centrum (POR), load induced spinal canal narrowing (LICN), maximum hoop strains, and location of maximum radial displacement.

Tumor size was varied in the model to encompass 0% (intact), 15%, 30% or 45% of the trabecular bone volume. Results for the metastatically involved models loaded to –800N at 16000 N/s were compared to the intact model under the same loading configuration. Introduction of a 15% tumor into the spinal motion segment model increased the LICN by over a factor of 2 and vertebral pore pressure by 46%. A 30% tumor, increased the LICN by 250% and caused a 116% increase in vertebral pore pressure. A 45% tumor increased the LICN by 509% as compared to the intact model accompanied by a 198% increase in pore pressure in the vertebral centrum. Similarly, larger tumor size caused marked increases in tensile hoop strains at the midline of the anterior vertebral body wall; inclusion of a 45% tumor caused a 278% increase in tensile hoop strain. Moreover, location of maximum radial displacement shifted from an area adjacent to the endplate in the intact model to the midline of the posterior vertebral body wall in the metastatically involved models.

An increase in the axial compressive load applied to the model of 50% increased the LICN by approximately 60% in the intact, 15%, 30% and 45% tumor analyses. The percentage increase in pore pressure generated by a 50% increase in load declined from 88% in the intact model to 49% in the model with 45% tumor involvement.

The apparent density of the trabecular bone in the model was varied from 0.10 g/cm^3 to 0.17g/cm^3. This 70% increase in the apparent density of the trabecular bone, caused a 157% reduction in LICN and a 63% reduction in the tensile hoop strain in the 15% tumor model. Metastatic involvement of osteoporotic trabecular bone yielded a higher burst fracture risk than denser bone under the same loading configuration.

Similar to results from the 2D axisymmetric model, the greatest effects on LICN, vertebral pore pressures and tensile hoop strains occur from an increase in tumor size. The amount of metastatic involvement of the vertebral body is the most important determinant of burst fracture risk. Increases in the applied load were also found to increase the risk of burst fracture patterns in the metastatically involved spine, thus patients' weight and anticipated activity level will also be important factors for clinicians to consider in determining a patients' course of treatment. Increases in tensile hoop strains and canal narrowing also have important implications for an increased risk of neurologic compromise in patients with reduced vertebral bone densities. Clinically, our data suggest that bone mineral density may be an important predictor of burst fracture risk and neurologic injury in patients with vertebral metastases. Failure of the vertebra due to elevated tensile hoop strains would correspond to clinical patterns seen in the burst fracture of metastatically involved vertebral bodies in which pieces of bone and tumor tissue may be retropulsed into the spinal canal. Further analyses are being run to examine the effects of disc degeneration,

pedicle involvement and faster rates of loading. A limitation of this procedure is the length of time (approximately 48 hours) required for a single run of the model, however all additional runs needed to complete our parametric analyses should be completed within the next six weeks.

Task 5: Identify parameters which can be used as a basis for modeling validation of metastatically involved vertebral bodies.

In order to validate the model, analyses were conducted under conditions which could be carried out in the experimental testing. The intact and the 15% tumor model were loaded in axial compression with a pressure of -0.62 or -0.93 MPa at a loading rate of 3200, 16000 or 32000 N/s. These loads approximate the compressive force on the lumbar spine for an individual standing upright, holding a 3.8 kg or 8.3 kg mass with outstretched arms (4) respectively. We considered three main outcome variables: the load induced spinal canal narrowing (LICN), the hoop strain (ε_h) at the midline of the anterior vertebral body wall and the pore pressure (POR) generated in the vertebral centrum. The results from these analyses are compared to the experimental data in Task 7.

Technical Objective 4: CT scan models

Task 6: Develop a specimen-specific finite element model from a vertebral body CT scan to examine the validity and applicability of the generalized poroelastic finite element model. Compare these results to experimental data derived from axial compressive loading of the specimen in task 7.

A CT scan was taken of one of the spinal motion segments prior to experimental testing. From this CT scan data a three-dimensional finite element mesh is in the midst of being constructed which will incorporate variation in the material properties of the vertebral bone. Aggregate modulus and hydraulic permeability values for each element is based on the bone density measurements from the CT scan. Intervertebral discs will be attached to the vertebral model to provide appropriate loading conditions, similar to the idealized model. The model will likewise be loaded in axial compression through the midplane of the superior intervertebral disc to 0.62 MPa and 0.93 MPa. A second model with a defect corresponding to the cored area removed in the experimental testing (Task 7) will be analyzed as well. This specimen-specific model will focus on trabecular bone failure and the potential for neurologic deficit, utilizing the same outcome variables as the idealized model: LICN, ε_a, ε_h and POR. The results from this model will be compared to the idealized model and the experimental testing of the spinal motion segment. This protocol will serve as a basis to determine whether patient specific finite element modeling can provide significantly better prediction of the risk of burst fracture and neurologic compromise in the metastatically involved spine as compared to the parameters determined via the idealized modeling.

Technical Objective 5: Validation through mechanical testing

Task 7: Rate-sensitive mechanical testing of metastatically involved vertebral bodies and healthy vertebral bodies with incorporated defects containing tumor tissue properties to validate modeling results.

Fresh-frozen spinal motion segments were harvested from 12 cadaveric spines through the midplane of the 12^{th} thoracic and 2^{nd} lumbar vertebrae. Bone mineral densities were determined for all specimens using DEXA in the lateral projection. The spinal motion segments were tested in axial compression using a servo-hydraulic MTS machine (Figure 3). Specimens were put under a -100 N preload followed by a load of -800 or -1200N applied to the specimen at a rate of 3200, 16000 or 32000 N/s.

Following testing of the intact specimen a defect was introduced into the trabecular centrum of L1 (Figure 2b). A 16 mm diameter hole was cored into the trabecular centrum through the lateral wall, without breaking through the opposing cortex. The core was removed from the centrum and the defect filled with a 0.5% solution of agarose gel. This gel was formulated to mimic the average material properties of lytic tumor in bone. The core was dissected to yield an end-cap of trabecular bone and cortical shell which was reattached to the vertebral body using PMMA, filling all gaps for a tight seal. The defects occupied approximately 15% of the trabecular bone centrum by volume. Biomechanical testing of the specimens containing these defects was repeated as described above. Trabecular bone apparent densities were determined from the bone cores removed. We measured, under each loading configuration, the same outcome variables as described in Task 5: the load induced spinal canal narrowing (LICN), the hoop strain

(ε_h) at the midline of the anterior vertebral body wall and the pore pressure (POR) generated in the vertebral centrum.

The experimental results demonstrated an increase in LICN from 64% to 400% (232±107%) when a 15% tumor was included as compared to the intact specimens. This percentage change in LICN was found to increase as bone mineral density decreased (Figure 2). Tensile hoop strains along the midline of the anterior wall also increased with the inclusion of a tumor from 146% to 1067% (518±338%). This percentage change in tensile hoop strain similarly increased with decreasing bone mineral density.

In comparing the intact and 15% tumor finite element models, our poroelastic finite element model predicted a 104% increase in LICN with the inclusion of the tumor as compared to the intact model with a trabecular bone apparent density of 0.10 g/cm^3. When the trabecular bone apparent density was increased to 0.17 g/cm^3 the model predicted an 83% increase in LICN. In comparing bone density to canal narrowing, similar to the experimental results, lower bone density values predicted higher percentage increases in canal narrowing with the inclusion of the vertebral defect.

A 70% increase in the apparent density of the trabecular bone, caused a 157% reduction in LICN and a 63% reduction in the tensile hoop strain in the 15% tumor model. Similarly, in the experimental testing of the metastatically involved specimens, a 70% increase in bone mineral density yielded a reduction of 163% in LICN and a decrease of 217% in tensile hoop strain.

Inclusion of a metastatic defect into the vertebral body increases both narrowing of the spinal canal and tensile hoop strains at the vertebral midline. Decreasing vertebral bone density was found to increase the narrowing of the spinal canal and tensile hoop strains at the vertebral body midline in both the model and experimental testing. Our idealized model was found to serve as a good predictor of both changes in canal narrowing and tensile hoop strains as compared to our experimental data.

Technical Objective 6: Develop guidelines for prophylactic treatment of metastatically involved vertebral bodies

Task 8: Generate a set of guidelines to permit clinicians to select appropriate patients with vertebral body metastases for intervention before the development of neurologic compromise.

Ultimately the goal of this research is to develop parameters which can be used by clinicians to quantify the risk of fracture and neurologic compromise in patients with vertebral body breast cancer metastases. Through currently used imaging modalities, the size and location of a vertebral body tumor, pedicle involvement, vertebral body size, bone density and disc quality can all be determined. Following the completion of the parametric studies of our three-dimensional finite element model, our data will define the variables that put patients at the greatest risk for burst fracture and neurologic compromise. This will allow us to evaluate the risk of burst fracture and neurologic compromise under loads corresponding to activities of daily living. A factor of safety will be determined based on these criteria and their prioritization, which if below 1 will identify patients requiring clinical intervention. The identified parameters will serve as a basis for clinical guidelines for prophylactic treatment of metastatically involved vertebral bodies, using information available from CT scans and MRIs of individual patients. Our factor of safety parameter will be compared to patient specific data obtained through Mount Zion cancer center in a retrospective chart study to determine its potential clinical effectiveness. Prediction of which metastatic breast cancer lesions in the spine pose the greatest potential for neurologic compromise in a patient will provide a basis for appropriate clinical intervention.

Conclusion

I intend to complete the final stages of this project within the next 3 months, leading to my PhD in Bioengineering. Following this, I plan to continue to investigate metastatic breast cancer in order to develop an understanding of the mechanisms involved in the interaction between tumor and bone. I hope to apply this understanding both to clinical applications for treating metastatic breast cancer and ultimately to the prevention of the metastasis of breast cancer to bone. I have recently accepted a faculty research position at the University of Toronto in the Division of Orthopaedic Surgery at Sunnybrook Hospital. I believe with the experience I have gained through this project in computer modeling, mechanical testing, materials analysis and biomechanical theory applied to tumor tissue, following the completion of my doctoral studies I will be well equipped to pursue independent research in the field of metastatic breast cancer research.

REFERENCES:

1. Berry, J. M. Moran, W. S. Berg and A. D. Steffee, 1987, "A morphometric study of human lumbar and selected thoracic vertebrae," *Spine*, 12(4): p. 362-367.

2. Constans, E. deDevitiis, R. Donzelli, R. Spaziante, J. F. Meder, C. Haye, 1983, "Spinal Metastases with Neurologic Manifestations Review of 600 Cases," *Journal of Neurosurgery*, 59: p. 111-118.

3. Fredrickson, Edwards W.T., Rauschning W., Bayley J.C., Yuan H.A., 1992, "Vertebral burst fractures: an experimental, morphologic, and radiographic study.", *Spine*, 17(9): p. 1012-1021.

4. Schultz, Andersson G., Ortengren R., Haderspeck K., Nachemson A., 1982, "Loads on the lumbar spine.", *Journal of Bone and Joint Surgery* , 5: p. 713-720.

5. Whyne, Hu SS, Klisch S, Lotz JC. Effect of the Pedicle and Posterior Arch on Vertebral Body Strength Predictions in Finite Element Modeling., *Spine*, 1998 23(8): 899-907.

6. Wong, V. L. Fornasier, and I. MacNab, 1990, "Spinal Metastases: The Obvious, the Occult, and the Impostors," *Spine,* 15(1): p. 1-3.

APPENDIX A: FIGURES

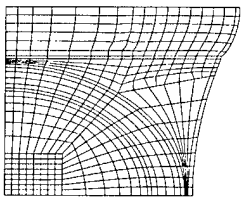

Figure 1: 2D Axisymmetric Finite Element Model of a Metastatically Involved Spinal Finite Element Model

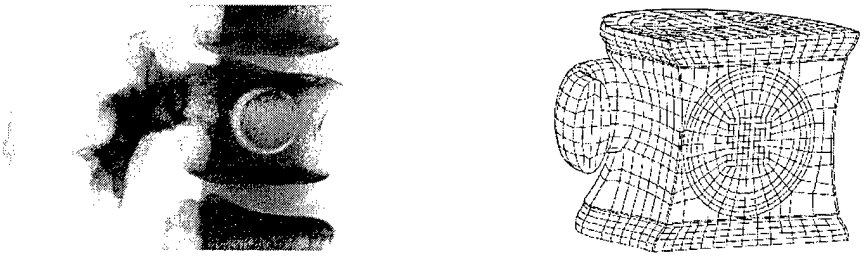

Figure 2: **(a)** Xray of a Spinal Motion Segment with an Artificially Introduced Defect **(b)** 3D Poroelastic Metastatically Involved Vertebral Body Finite Element Model with adjacent intervertebral discs.

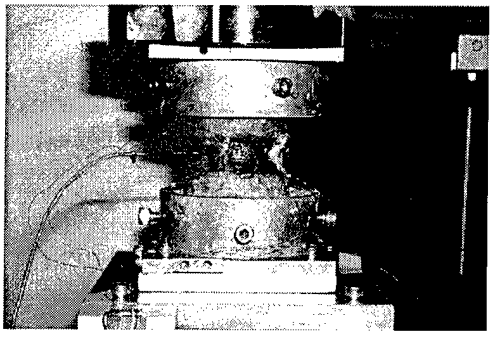

Figure 2: Experimental set-up for axial compressive testing of a Spinal Motion Segment with an Artificially Introduced Defect

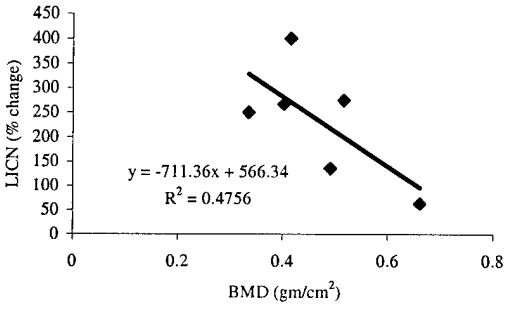

Figure 3: Bone Mineral Density vs. % Change in Canal Narrowing between the Intact and Metastatically Involved Vertebral Bodies – Experimental data.

APPENDIX B: KEY RESEARCH ACCOMPLISHMENTS

- Developed an experimental protocol to analyze biphasic material properties of very soft hydrated tissues.

- Determined the mechanical properties of lytic bone metastases.

- Our results showed a relationship between tumor cellularity and the material parameters aggregate modulus and hydraulic permeability. Tumors with greater cellularity were found to demonstrate higher hydraulic permeabilities and lower aggregate moduli than less cellular tumors.

- Demonstrated the importance of utilizing poroelasticity in modeling the metastatically involved spine.

- Parametric analyses of the 2D axisymmetric finite element model have yielded the following results:
  - Faster loading rates were shown to indicate an increased likelihood for endplate failure in intact vertebral bodies in concurrence with clinical observations.
  - Increased tumor size was found to cause the greatest increase in metastatically involved vertebral body displacements, strains and pore pressure and suggests a greater risk for endplate and radial vertebral body failure as the size of the defect increases.
  - Higher loading rates applied to the metastatically involved models indicates an escalating risk of a potential burst fracture pattern
  - Variation of tumor tissue material properties does not have a large effect in assessing failure risk.

- Constructed and validated a three-dimensional poroelastic finite element model of a metastatically involved spinal motion segment.

- Inclusion of a metastatic defect into the vertebral body was shown to increase both narrowing of the spinal canal and tensile hoop strains at the vertebral midline under axial compressive loading. Inclusion of a tumor changed the location of maximum radial displacement on the vertebral cortex from adjacent to the endplate to the posterior wall vertebral midline, which may correspond to a shift from a compression fracture pattern to a burst fracture pattern.

- Tumor size is the most important factor in determining the risk of burst fracture and potential for neurologic deficit in the metastatically involved spine.

- A decrease in vertebral bone density was found to increase the narrowing of the spinal canal and tensile hoop strains at the vertebral body midline. This suggests that bone mineral density may be one important predictor of burst fracture risk and neurologic injury in patients with vertebral metastases.

- Higher rates of loading were shown to increase the pore pressure generated in the vertebral centrum corresponding to an elevated risk of burst fracture.

- The application of higher loads to the spine increased both vertebral pore pressures, tensile hoop strains, and spinal canal narrowing, thus a patient's weight and activity level are important considerations in estimating burst fracture risk.

- The posterior arch provides support to the posterior wall of the vertebral body. Metastatic involvement of the pedicle can compromise the posterior arch causing increases in both maximum strains and radial displacement of the posterior vertebral body wall (5).

- Determined that the mechanism of fracture in the metastatically involved spine is due to pressurization of the vertebral body and elevated tensile hoop strains. This would correspond to burst fracture patterns seen clinically with a risk of neurologic compromise due to retropulsion of bone and tumor into the spinal canal.

APPENDIX C: REPORTABLE OUTCOMES

Publications:
Whyne, C., Hu, S.S., Klisch, S., Lotz, J.C., Effect of the Pedicle and Posterior Arch on Vertebral Body Strength Predictions in Finite Element Modeling., *Spine*, 1998 23(8): 899-907.

Whyne, C., Hu, S.S., Lotz, J.C., The effect of tumor size, material properties and loading rate on the compressive response of metastatically involved vertebral bodies., 25th Annual Meeting of the International Society for Study of the Lumbar Spine, Brussels, Belgium, June 1998.

Whyne, C., Hu, S.S., Lotz, J.C., Vertebral Body Modeling: The Effects of Poroelasticity and Loading Rate, Forty-Fourth Annual Meeting of the Orthopaedic Research Society, March 1998.

Whyne, C., Hu, S.S., Lotz, J.C., Poroelastic Finite Element Modeling of Metastatically Involved Vertebral Bodies., Forty-Fourth Annual Meeting of the Orthopaedic Research Society, March 1998.

Abstracts in Submission:
Whyne, C., Hu, S., Workman, K., Lotz, J., Mechanical Properties of Metastatic Tumors in Bone. Forty-Fifth Annual Meeting of the Orthopaedic Research Society, March 2000.

Whyne, C., Hu, S., Lotz, J., The Effect of Bone Density on the Metastatically Involved Spine: Three-Dimensional Finite Element Modeling and Experimental Validation. Forty-Fifth Annual Meeting of the Orthopaedic Research Society, March 2000.

Manuscripts in Preparation:
A Parametric Study of Metastatically Involved Vertebral Bodies using Poroelastic Finite Element Modeling.

Characterization of the Mechanical Properties of Metastatic Tumors in Bone.

Dissertation: Development of guidelines for the prophylactic treatment of metastatically involved vertebral bodies

Other Presentations:
The Biomechanics of Burst Fracture: Cancer in the Spine. Ryerson Polytechnic University, Toronto Canada. March 9, 1999.

Academic Degree Supported by this Award:
PhD, Bioengineering
University of California, Berkeley/ University of California, San Francisco
Expected Graduation Date: November 1999

Future Employment / Research Opportunities:
Job Offer: Scientist, Orthopaedic Bioengineering Laboratory and Assistant Professor, Department of Surgery, Sunnybrook Hospital, University of Toronto. Toronto, Canada.
Employment Accepted.
Start Date: January, 2000.
This position offers me a wonderful opportunity to continue my focus investigating bone metastases resulting from primary breast neoplasms and other cancers. Sunnybrook Health Science Centre combines a strong Orthopaedic Department and an top notch Cancer Centre, which makes it an ideally suited environment for my continued focus on the biomechanics of tumor and bone.

Job Offer: Assistant Professor, Department of Mechanical Engineering, Ryerson Polytechnic University. Toronto, Canada.
Offer not accepted.

SPINE Volume 23, Number 8, pp 899-907

Effect of the Pedicle and Posterior Arch on Vertebral Body Strength Predictions in Finite Element Modeling

Cari M. Whyne, BSc,*† Serena S. Hu, MD,*† Stephen Klisch, MS,* and Jeffrey C. Lotz, PhD*†

Study Design. A finite element study to predict the contribution of the pedicles and the posterior arch to vertebral body strength.

Objective. To determine the effect of the pedicle and posterior arch on strain distributions occurring within the vertebral body under axial compressive loading.

Summary of Background Data. Posterior vertebral body fracture can arise from high-impact or normal loading in bones compromised by osteoporosis or neoplasm and can result in spinal canal encroachment. Anatomically, the pedicles and posterior arch have a potential role as a structural buttress to the posterior vertebral body wall. However, most finite element models used to investigate vertebral body strength have neglected these structures.

Methods. Three 3-dimensional finite element models were developed of L1, incorporating anatomic curvature, with varying degrees of posterior element inclusion (no pedicle, pedicle, and pedicle and posterior arch). Three cases were analyzed with each model: 25% dehydrated disc, normal healthy disc, and uniform pressure loading. Outcome variables were the maximum von Mises strains and the displacement of the posterior wall into the spinal canal.

Results. Inclusion of the posterior arch resulted in substantial decreases in maximum strain and posterior wall displacement under all loading configurations using transversely isotropic trabecular bone properties. No changes in maximum strains or displacements were recorded in the pedicle model, compared with that observed in the no-pedicle baseline case.

Conclusions. The pedicle functions as a structural buttress, providing support to the posterior wall of the vertebral body when constrained through the posterior arch. To yield more accurate vertebral body strength predictions from finite element modeling, the posterior arch should be included. [Key words: finite element analysis, pedicle, posterior arch, strength predictions, vertebral body] **Spine 1998;23:899-907**

From the *Orthopaedic Bioengineering Laboratory, Department of Orthopaedic Surgery, University of California San Francisco, and the †University of California Berkeley–University of California San Francisco Joint Graduate Group in Bioengineering, San Francisco, California.
Acknowledgment date: December 17, 1996.
Acceptance date: June 9, 1997.
Device status category: 1.

The incidence of vertebral body fracture in the United States is estimated to be more than 500,000 per annum.[20] This rate is expected to increase as the population continues to age and osteoporosis becomes more prevalent. Fracture prediction has significant clinical importance, in that prevention of fracture in high risk patients is often possible through prophylactic intervention, by external bracing or by internal stabilization.[5,12] Methods of vertebral body strength prediction developed by biomechanical testing and mathematical models can be used to assess vulnerable areas in the vertebral body and may in the future be used to form clinical guidelines for intervention.

Although most vertebral body fractures occur anteriorly, posterior vertebral body (burst) fractures can be caused by high-impact loading or normal loading in bones compromised by neoplasm. Because of the proximity to the spinal cord and nerve roots, posterior body fracture can cause bone or tumor to encroach on the spinal canal, resulting in potentially irreversible neurologic injury. Symptoms may include paralysis, loss of sensation, and loss of bowel and bladder function and may result in a significant decline in quality of life. There are approximately 18,000 new cases of metastatic involvement of the vertebral body per year in the United States, often resulting in vertebral instability.[1] From 5% to 10% of cancer patients have spinal metastases resulting in neurologic manifestations.[4] Longer survival times for patients with metastatic cancer have increased the incidence of pathologic fracture.

Anatomically, the pedicles have a potential role as a structural buttress, providing support through their attachment to the posterior wall of the vertebral body. Pedicle erosion is present in approximately 75% of patients requiring surgical decompression for symptomatic spinal metastases and may be the first radiographic sign of spinal instability.[19] Destruction of one or both pedicles on a vertebral body is seen clinically to increase the likelihood of neurologic compromise, implying that the status of the pedicles may be important in assessing burst fracture risk. However, most finite element models used to investigate vertebral body strength neglect this structure.[15,24,25] As a result, the roles of the pedicles and

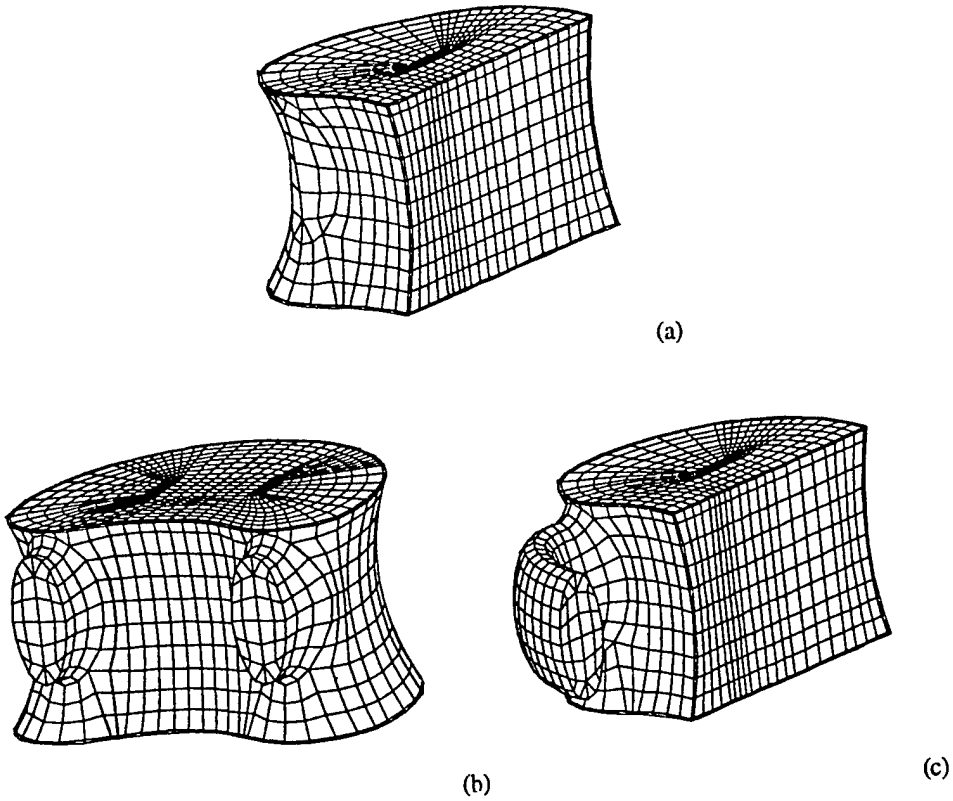

Figure 1. Finite element model of the first lumbar vertebra: **a**, no-pedicle model; **b**, full vertebral body representation of the pedicle segment model (generated with sagittal symmetry from the half vertebral body model used in the analyses); **c**, symmetric model with the inclusion of the posterior arch.

the posterior arch in vertebral body strength have not yet been determined analytically. The objective of the current study is to use finite element modeling to determine the effect of the pedicle and posterior arch on the strain distributions occurring within the vertebral body under axial compressive loading.

■ Methods

A three-dimensional finite element model of a lumbar vertebra was developed that was symmetric in the sagittal plane and incorporated anatomic vertebral body curvature based on average values reported for L1.[2] Asymmetry of the vertebral body was represented in both the anteroposterior and inferosuperior directions, although the biconcavity of the endplates was not included. In the horizontal plane, the posterior vertebral body was modeled as concave, representing the anterior wall of the spinal canal (Figure 1A).

The mesh consisted of 4200 elements (8-noded bricks and 6-noded wedges) and was generated and analyzed using commercial software (PATRAN 5.0, PDA Engineering, Costa Mesa, CA; and ABAQUS 5.5, HBK Inc., Pawtucket, RI). A second model was generated that was identical to the first with the exception that a pedicle segment was included (Figure 1B). The pedicle was modeled as elliptical to a distance of 3.5 mm and attached with a 1.5-mm radius of curvature to the posterior vertebral body.[2,16] The cortical thickness of the pedicle was taken as 30% of the major dimension and 40% of the minor dimension.[16] There were no boundary conditions imposed on the free end of the pedicle. A third model extended the pedicle segment to form the posterior arch and incorporated boundary conditions of sagittal symmetry[2] (Figure 1C). No other posterior structures were modeled. No convergence study was performed on the model, because the degree of mesh refinement used has been demonstrated to be adequate in previous similarly sized models.[24]

All materials were assumed linearly elastic and homogeneous and designed to represent a middle-aged vertebral body (approximately 60) years old).[17] The cortical shell of the vertebral body and cortical shell of the pedicle were modeled isotropically with elastic moduli of 5,000 MPa and 12,000 MPa respectively. The cortical endplate was modeled isotropically with an elastic modulus of 1,000 MPa. The trabecular bone of the centrum was modeled as transversely isotropic (at every point in the material the mechanical properties in the horizontal plane are equal in all directions), with an elastic modulus of 60 MPa in the inferosuperior direction and one third that value (20 MPa) in the transverse direction.[17] The shear modulus in the inferosuperior direction was taken as 15.4 MPa, twice the value in the transverse plane (7.7 MPa).[24] Analyses were also performed modeling the trabecular bone as isotropic with an elastic modulus of 60 MPa. The Poisson's ratio (a measure of lateral strain relative to axial strain) was assumed to be 0.3 for all bone ($\nu = \nu_{12} = \nu_{13} = \nu_{23} = 0.3$). Additional runs were performed using a reduced Poisson's ratio of 0.1 for the trabecular bone (with isotropic and transversely isotropic properties) to determine the effect of Poisson's ratio on the contribution of the pedicle. Values of the Poisson's ratio greater than 0.3 were not considered, because the resulting combinations of material constants violated basic thermodynamic constraints. In the model without the pedicle, the cortical shell covered the pedicle attachment sites, a similar configuration to other previous finite element models.[15,24]

To examine how varied loading configurations may alter the effect of the pedicle and posterior arch, the model was

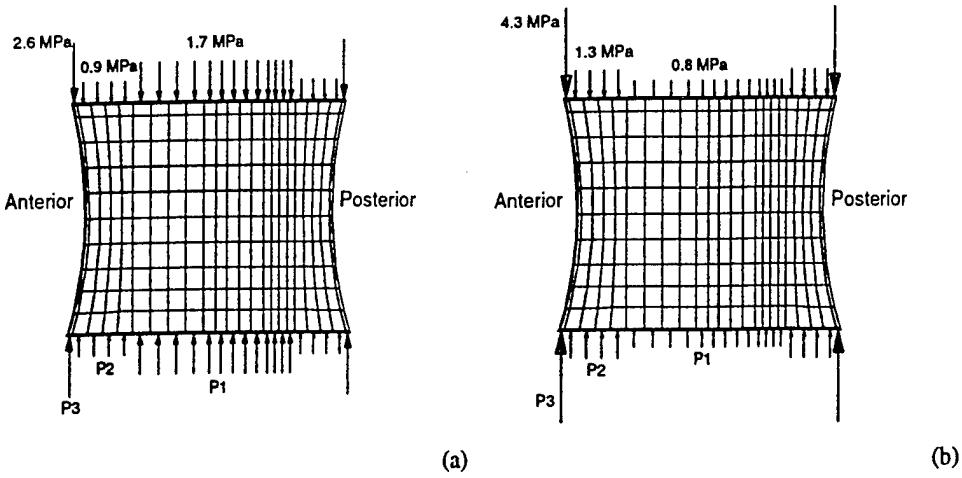

Figure 2. Loading configurations of the vertebral body model—sagittal view: **a**, normal healthy disc; **b**, 25% dehydrated disc. The pressures were applied to three zones corresponding to an inner region under the nucleus pulposus (P1), a mid area adjacent to the anulus fibrosis (P2), and an outer ring corresponding to a region occupied by the cortical shell (P3).

axially loaded using three boundary conditions: 1) a uniform pressure loading of 1.24 MPa; 2) a pressure loading of the same magnitude applied as if through a normal healthy disc[10]; and 3) a pressure loading representing a 25% dehydrated disc[10] (Figure 2). These correspond to a 1600-N force applied to the whole vertebral body and approximate the compressive force on the lumbar spine for an person standing upright, holding a 13-kg mass with outstretched arms.[21] The inferior and superior vertebral body surfaces were divided into three regions of pressure loading: an inner region under the nucleus pulposus (P1), a mid area adjacent to the anulus fibrosis (P2), and an outer ring corresponding to a region occupied by the cortical shell (P3). For the healthy disc, the pressure on the inner region was almost twice that on the region adjacent to the anulus (P1 = 1.7 MPa; P2 = 0.9 MPa; and P3 = 2.6 MPa). For the dehydrated disc, increased pressure was shifted toward the periphery with higher pressure loading in the regions adjacent to the anulus and the cortical shell (P1 = 0.8 MPa; P2 = 1.3 MPa; and P3 = 4.3 MPa). The uniform pressure loading was applied to the model (P1 = P2 = P3 = 1.24 MPa) for two separate cases: first using transversely isotropic properties to model the trabecular bone, as was done for the other loading configurations, and then adjusting the model to include only isotropic trabecular bone properties. Pressure loading on the inferior endplate was adjusted proportionally to the same absolute magnitude applied to the superior endplate to ensure static equilibrium.

Overall, four cases were analyzed in each of the no-pedicle, pedicle, and posterior arch models: 1) 25% dehydrated disc loading, 2) normal healthy disc loading, 3) uniform pressure loading (with transversely isotropic trabecular bone properties), and 4) uniform pressure loading (with isotropic trabecular bone properties). As well, the no-pedicle model was run with isotropic trabecular bone properties under the 25% dehydrated and normal healthy disc loading configurations. Under uniform pressure loading, trials were run with a reduced trabecular bone Poisson's ratio with isotropic and transversely isotropic properties. Outcome variables were the magnitude of the maximum von Mises strain and the displacement of the posterior wall toward the center of the spinal canal. Locations of maximum strains were also identified, visualized on the sagittal plane corresponding to the axis of symmetry, and verified by considering transverse and vertical slices through the model at the midlines of the pedicle attachment sites.

■ Results

Including the posterior arch decreased the peak von Mises strains within the vertebral body by approximately 33% from the baseline case (no-pedicle) in all three loading conditions (degenerated disc, 26%; normal disc, 24%; and uniform pressure, 33%; Table 1A). Concomitant with this was a shift in the location of peak strain from near the posterior vertebral body wall toward the vertebral centrum (Figure 3). The intact posterior arch also reduced the rearward deformation of the posterior body wall (degenerated disc, 26%; normal disc, 44%; uniform pressure, 43%; Table 1B; Figure 4). Including the pedicle (without the posterior arch) had no significant effect on either the peak strains or posterior vertebral body displacements.

Table 1. Maximum von Mises Strains in the Vertebral Body for Each Model Comparing Results With Transversely Isotropic Versus Isotropic Trabecular Bone Properties and Percent Change in Strain From the Posterior Arch to the No-Pedicle Baseline Case

	25% Dehydrated Disc		Healthy Disc		Uniform Pressure	
	Transversely Isotropic	Isotropic	Transversely Isotropic	Isotropic	Transversely Isotropic	Isotropic
No-pedicle	0.0233	0.0240	0.0358	0.0324	0.0273	0.0251
Pedicle segment	0.0232		0.0358		0.0274	0.0253
Posterior arch	0.0185		0.0288		0.0205	0.0241
% change	26		24		33	4%

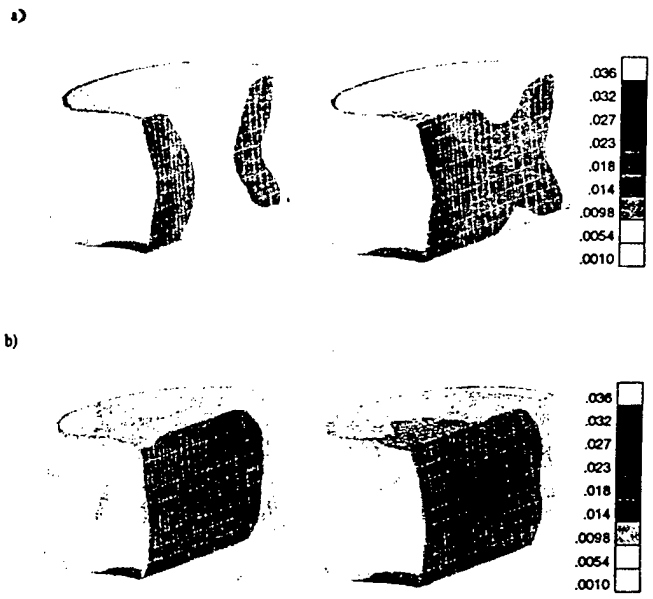

Figure 3. Von Mises strain distributions: **a**, 25% dehydrated disc (transversely isotropic trabecular bone) with the posterior arch and without the pedicle; **b**, normal healthy disc (transversely isotropic trabecular bone) with the posterior arch and without the pedicle. Including the posterior arch caused a decrease in the peak von Mises strain by 26% in the 25% dehydrated disc case and by 24% in the normal healthy disc case.

When the trabecular bone was represented as isotropic (as opposed to transversely isotropic), the peak von Mises strains were minimally affected in the no-pedicle and pedicle models (degenerated disc, +3%; normal disc, −10%; uniform pressure, −9%; Table 1A), whereas the posterior vertebral body wall displacements decreased by between 130% and 170% (Table 1B). When the posterior arch was included and uniform pressure applied, the isotropy assumption had a moderate effect on the peak strains (−15%; Table 1A), accompanied by a large reduction in posterior wall displacement (123%; Table 1B).

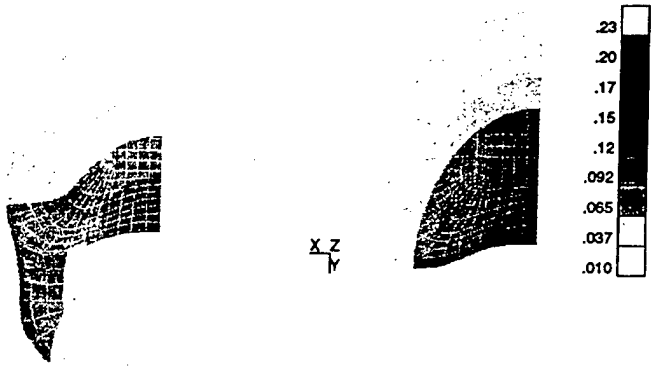

Figure 4. Displacement (mm) of the vertebral body in the posterior (y) direction (toward the center of the spinal canal) for the 25% dehydrated disc loading configuration with the posterior arch (left) and without the pedicle (right) (magnification, ×1). The model without the pedicle demonstrates a 34% greater displacement into the spinal canal.

The magnitude of the peak von Mises strain and posterior vertebral body wall displacement declined with the reduction of the Poisson's ratio from 0.3 to 0.1 (Table 2), whereas the strain pattern remained largely unchanged. With this reduction in the Poisson's ratio, inclusion of the posterior arch caused a slight (4%) reduction in the peak strain when transverse isotropy was assumed, and no change when isotropy was assumed (Table 2). Also, when the Poisson's ratio was decreased under uniform pressure loading, the posterior wall displacement declined by 40% and 23% for the transversely isotropic and isotropic cases, respectively (Table 2).

In the pedicle model, the displacement of the free end of the pedicle was between 0.14 and 0.21 mm in the lateral direction (Figure 5). With the assumption of trabecular bone isotropy, this displacement was reduced to 0.8 mm.

■ Discussion

The study was designed to determine the influence of the pedicle and posterior arch on vertebral body strain distributions under axial compressive loading. Inclusion of the posterior arch resulted in significant changes in three outcome variables. First, a decrease was noted in the peak von Mises strains of between 24% and 33% from the baseline no-pedicle case. Second, addition of the posterior arch shifted the location of maximum von Mises strain away from the posterior vertebral body wall and toward the vertebral centrum. Third, the displacement of the posterior vertebral body toward the spinal canal was reduced by between 34% and 44%, depending on the assumptions regarding the intervertebral disc. The greatest effect was demonstrated with the trabecular bone represented as transversely isotropic with a Poisson's ratio of 0.3 (Table 3).

These structural consequences for the vertebral body are related to constraints on the displacement of the pedicle created by the posterior arch. When the pedicle only was modeled, no significant changes in vertebral body strain were noted when compared with the baseline case, which suggests that the mere presence of the pedicle on the posterior vertebral body wall does not affect vertebral body strains significantly. Importantly, the pedicle model demonstrated that, in response to vertebral body compression, the pedicle has a natural tendency to displace laterally. When the posterior arch is included, this displacement is constrained, which results in a bending moment in the horizontal plane, generated in the posterior vertebral body wall (Figure 6). This bending moment, in turn, causes a decrease in the posterior displacement of the vertebral body cortex adjacent to the spinal canal.

The magnitude of the influence of the posterior arch is dependent on material property assumptions for the ver-

Table 2. Displacements of the Posterior Wall (mm) Toward the Spinal Canal

	25% Dehydrated Disc		Healthy Disc		Uniform Pressure	
	Transversely Isotropic	Isotropic	Transversely Isotropic	Isotropic	Transversely Isotropic	Isotropic
No-pedicle	0.23	0.098	0.32	0.12	0.28	0.11
Pedicle segment	0.23		0.32		0.28	0.11
Posterior arch	0.17		0.23		0.20	0.087
% change*	34		44		43	27%

* The reduction of posterior displacement found with inclusion of the posterior arch.

tebral body trabecular bone. Given the primary mechanism by which the arch appears to affect posterior cortex displacement—constraining lateral displacement of the pedicle—factors that decrease the tendency for the pedicle to move laterally, will diminish the influence of the arch. As would be expected, when the stiffness in the transverse plane is increased by imposing isotropy (from 20 MPa to 60 MPa), the transverse strains, and thus posterior vertebral body wall displacement, are decreased by between 20% and 60%. Accordingly, the posterior arch had a diminished effect on the peak vertebral body strain when trabecular bone was modeled as isotropic (5% *versus* 22%). However, inclusion of the posterior arch continued to have a significant effect on the displacement of the posterior vertebral body wall (a 20% decrease when the arch is included). Similarly, when the Poisson's ratio was decreased (from 0.3 to 0.1), the strains in the transverse plane, and therefore the contribution of the arch, were further reduced. Thus, the effect of the arch on vertebral body strains and posterior cortex displacement was minimized under the conditions of isotropy and a Poisson's ratio of 0.1 (17% decrease in displacement, compared with that in the no-pedicle case) and maximized under the assumption of transverse isotropy and a Poisson's ratio of 0.3 (29% decrease, compared with that in the no-pedicle case).

According to these results, the structural significance of the posterior arch is patient-specific. Although even in healthy people vertebral body trabecular bone is not isotropic, there is evidence that this anisotropy increases with aging.[18] Therefore, the current data imply that because preferential bone loss leads to a diminished stiffness in the transverse plane with aging, the importance of the posterior arch toward supporting the posterior vertebral wall will be amplified. By extension, it is expected that when the vertebral body is affected by tumor, the posterior arch has even greater significance in protecting the posterior vertebral body and in preventing spinal canal encroachment. However, age-related loss of trabecular interconnectivity may correspond to representation of the trabecular bone with a lower Poisson's ratio, reducing the role of posterior arch support.

A number of previously reported vertebral body finite element models used for fracture risk estimation have not incorporated the anatomic curvature of the vertebral body.[15,24,25] In both axis-symmetric and elliptical models, pure axial compressive loading and exclusion of the pedicle yields symmetric stress–strain patterns. When using anatomic vertebral body curvature, the endplate centroid is closer to the posterior vertebral body wall, compared with its location in axis-symmetric and elliptical models (Figure 7), resulting in an asymmetric stress–strain distribution as seen in the current model. The posterior location of the center of applied pressure in the anatomic case corresponds to the location of the region of maximum strain seen in the no-pedicle model under uniform pressure loading. This result demonstrates that the magnitude and location of peak strains are also dependent on vertebral body shape. The peak strain patterns found using isotropic trabecular bone properties

Table 3. Effect of Variations in Trabecular Bone Properties Under Uniform Pressure Loading Comparing Peak von Mises Strain Magnitudes (%) and Locations and the Posterior Vertebral Body Wall Displacement (mm) for Isotropic and Transversely Isotropic Representations of Trabecular Bone With Poisson's Ratios of 0.3 and 0.1 in the No-Pedicle and Posterior Arch Vertebral Body Models

		Peak von Mises Strain Magnitude	Peak von Mises Strain Location	Posterior Wall Displacement (mm)
Isotropic	$\nu = 0.3$	0.0251	Central (sup-post)	0.11
No-pedicle	$\nu = 0.1$	0.0244	Central (sup-post)	0.035
Isotropic	$\nu = 0.3$	0.0241	Central (sup-post)	0.088
Posterior arch	$\nu = 0.1$	0.0240	Central (sup-post)	0.029
Transversely isotropic	$\nu_{12} = \nu_{13} = \nu_{23} = 0.3$	0.0273	Posterior–central	0.28
No-pedicle	$\nu_{12} = \nu_{13} = \nu_{23} = 0.1$	0.0271	Central (sup-post)	0.096
Transversely isotropic	$\nu_{12} = \nu_{13} = \nu_{23} = 0.3$	0.0205	Central (posterior shift)	0.20
Posterior arch	$\nu_{12} = \nu_{13} = \nu_{23} = 0.1$	0.0261	Central (sup-post)	0.069

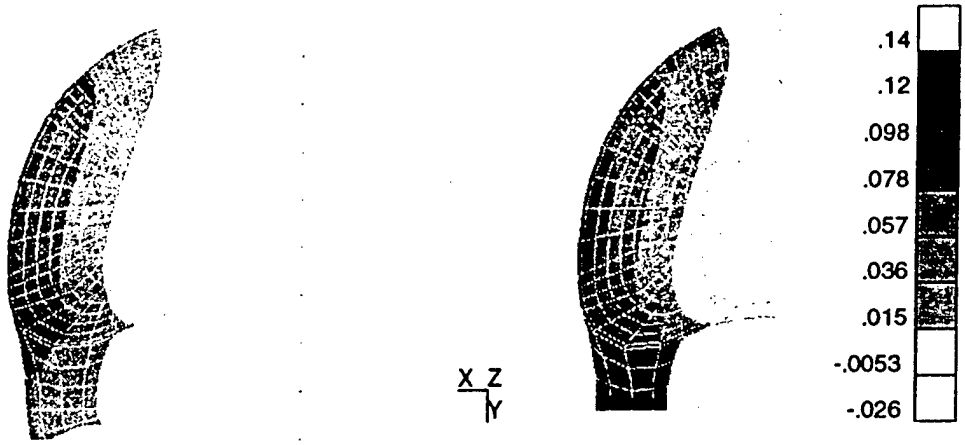

Figure 5. Displacement of the pedicle segments (mm) in the lateral (x) direction for the 25% dehydrated disc loading configuration in the posterior arch (left) and pedicle segment (right) models (magnification, ×1). The lateral displacement of the pedicle segment end is reduced from 0.14 mm to 0.03 mm with the inclusion of the posterior arch.

were centrally located and relatively symmetric, compared with patterns observed in cases using transverse isotropy. The anatomic vertebral body curvature has less of an effect on peak strains in the vertebral body when isotropic trabecular bone properties are modeled, yet still higher concentrations of strain are observed at the superior–posterior region of the sagittal plane, compared with strain values found in the other corners.

Another approach for assessing the contribution of the pedicle-toward-vertebral-body strength is through mechanical testing.[13–15,23,26] McGowan et al[14] and Silva et al[23] tested isolated vertebral body specimens under combined axial and flexion loads applied directly to the vertebral bodies through load platens parallel to the endplates. In both studies, the same protocol was used in comparing intact vertebral body strength with the strength of vertebral bodies with simulated metastatic defects. In these studies, fractures resulted at the anterior–superior endplate with evidence of collapse of the anterior vertebral body wall. In no case was the posterior vertebral body wall displaced into the canal, even in the vertebrae with defects. Silva et al[23] considered the effects of pedicle disruption on their loading configuration and reported that the absence of the pedicles (compared with specimens with an intact posterior arch) did not influence the strength of the vertebral bodies. However, posterior vertebral body fractures were not produced using their protocol, which may be because of the boundary conditions used. Given the current results, it is expected that the influence of the pedicle would become apparent experimentally in specimens loaded in pure compression through intact intervertebral discs.

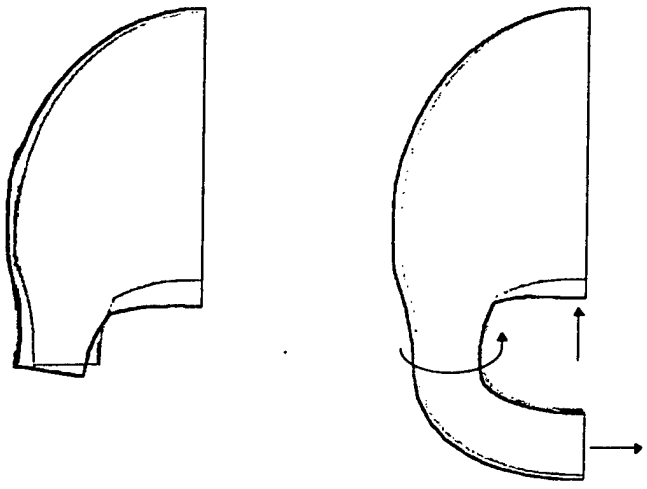

Figure 6. Axial compressive loading causes lateral displacement of the pedicle when no arch is modeled (left). The gray outlines represent the undeformed mesh and the black outlines the borders of the models under axial compressive loading. Displacement is seen as the difference between the outlines (magnification, ×5). The moment acting on the pedicle related to the constraints imposed by the posterior arch causes both a decrease in posterior wall displacement and lateral motion of the pedicle (right). This results in an overall reduction of von Mises strains in the vertebral body under axial compressive loading.

Burst fractures have been suggested to be caused by entry of the nucleus pulposus into the vertebral body through an endplate fracture, causing the body to pressurize and, ultimately, to burst.[7] Shirado et al[22] investigated the influence of disc degeneration on the mechanism of thoracolumbar burst fractures. Static axial compression of 11 motion segments (vertebra–disc–vertebra) resulted in seven typical burst fractures, with disruption of the middle endplate and herniation of the disc into the vertebral body. The endplate disruptions were located at the center or center posterior portions in all burst fractures, in segments with healthy and slightly degenerated discs. No burst fractures were seen in the specimens with severely degenerated discs. To confirm the stress state resulting in these burst fracture patterns, Shirado et al[24] also developed a two-dimensional finite element model of the motion segment (neglecting the posterior elements). With a healthy disc under axial com-

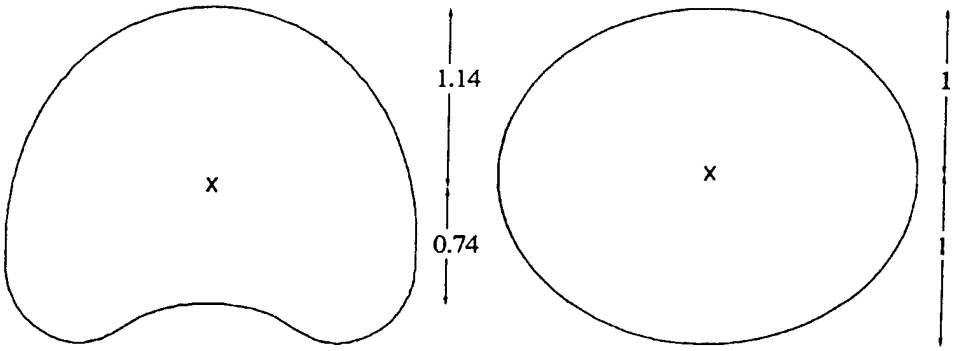

Figure 7. Centroids of the anatomic and elliptical vertebral body cross-sections. In the anatomic cross-section, the centroid is 26% closer to the posterior vertebral body wall than in the elliptical section.

pression, the highest stresses in the vertebral body were recorded in the center of the endplate, on the posterior wall, as well as in the trabecular bone under the nucleus pulposus. With a severely degenerated disc, the highest stresses occurred at the posterior cortex. These experimental data and the finite element model agree well with the current findings: The areas of maximum von Mises strain in this model (without the pedicle) correspond to the areas of maximum stress observed in their two-dimensional analysis. The current data, however, are described in terms of strain, rather than stress, to reduce the confounding effects of large variations in modulus in the description of failure properties of trabecular bone.[9]

The current results are limited by the use of linear elastic and homogeneous material properties. These assumptions reduce the complexity of the analysis but do not replicate the nonlinear postyield behavior of the vertebral body's trabecular bone.[11] However, loads were applied consistent with physiologic loading conditions in which overt failure is not expected to occur. Despite this, the results may potentially be extrapolated to investigate failure behavior, in that linear models have been successfully used previously to predict fracture of the proximal femur, which is also largely composed of trabecular bone.[11] As well, the rate of loading has been shown to have only very minor effects on the mechanical properties of trabecular bone under normal physiologic loading conditions,[3] and as such should not have a dramatic effect on the conclusions reached in the current models. Because of these idealizations however, the current results were used solely to make relative comparisons among the posterior arch, pedicle segment, and no-pedicle cases; and as such, the absolute value of the strain predictions may not have direct clinical relevance.

A further idealization in this model is the representation of the posterior arch as an extension of the pedicle, resulting in a constant cross-sectional area of the arch equal to that of the pedicle, which, at points, is larger than the actual anatomic cross-sectional area of the arch. Although this could exaggerate the effect of the posterior arch's constraint on the vertebral body, the anatomic representation of the posterior elements not included in this model (transverse and spinous processes) may compensate for this increased cross-sectional area.

A burst fracture is defined as the failure of the posterior wall of the vertebral body, usually resulting in some compromise of the spinal canal. In normal vertebral bodies, burst fractures may result from high-impact axial compressive loading, such as falls from heights and motor vehicle accidents. When pathologic processes affect the spinal column, posterior failure can occur with much reduced or even trivial loading. Older patient populations are more likely to be affected by such pathologic processes as disc degeneration, osteoporosis, or metastatic tumor involvement, which will increase the risk of vertebral body instability. In that pedicle erosion related to tumor involvement is present in approximately 75% of patients requiring surgical decompression for spinal metastases,[19] the current results may have particular clinical relevance to the occurrence of fracture of metastatically involved vertebral bodies in which one or both pedicles have been eroded by tumor. In addition, following a laminectomy, the posterior arch may be compromised, removing the sagittal constraint on the pedicle. As seen in the pedicle segment model, this compromise of the posterior arch causes an increase in both maximum von Mises strains and the displacement of the posterior vertebral body wall into the spinal canal. Although laminectomies are avoided where possible in patients with vertebral body lesions because of resultant increased instability and kyphosis, the increase in peak von Mises strains and further encroachment into the spinal canal caused by the disruption of the posterior arch may suggest an additional rationale for avoiding this procedure in such patients.

It is important to note that results based on the inclusion or lack of the pedicle in this model do not have a direct clinical correlation to the presence or absence of a pedicle *in vivo;* however, according to the current results, surgical procedures or pathologic processes that compromise the continuity of the posterior arch can significantly alter vertebral column strength. Finite element modeling, such as that carried out in this study, uses an idealized representation of a vertebral body, and thus specific results (predictions of strains and stresses) may not be generalizable to actual clinical cases. Rather, the strength of this approach lies in the use of such idealized models to isolate cause–effect correlations and to filter

out inherent variability found in experimental testing.[8] A further step toward clinical relevance would require experimental validation of the finite element vertebral body model, with and without the pedicles and the posterior arch.

In summary, in the current results, the posterior arch is shown to constrain the vertebral body, and therefore to decrease posterior vertebral body strain and cortex displacement. However, the extent of this influence is dependent on the material properties of the vertebral body and therefore may vary from patient to patient, depending on their bone and intervertebral disc quality. Additional studies are needed to verify these results experimentally and to investigate the influence of the posterior arch under a broader range of assumptions regarding vertebral body loading and trabecular bone quality. For instance, in the results presented here, it is suggested that when the vertebral body is compromised by a tumor, the presence of the posterior arch can be a substantial factor in preventing displacement of bone into the spinal canal. These observations, if proved true, should affect clinical decisions regarding the optimal surgical treatment of patients with metastatic involvement of the spine.

It is probably equally important to consider the forces transmitted into the posterior arch through the facet joints.[6] Although in the current results the stabilizing influence of the posterior arch is highlighted, large facet forces may induce significant strains in the posterior vertebral body. Thus, in addition to the vertebral body itself, the posterior arch and the forces transmitted through it should also be considered when a comprehensive technique for the prediction of vertebral body fracture is developed.

Despite these uncertainties, it is apparent from these results that the posterior arch should be included in finite element models developed for predicting vertebral body strength, particularly when burst fractures are of interest. To the extent that these theoretical results can be generalized to the clinical situation, clarification of the mechanism of interaction between the vertebral body and posterior arch will lead to improved decision making in the assessment and management of patients who have compromised spinal integrity.

References

1. Arguello F, Baggs RB, Duerst RE, Johnstone L, McQueen K, Frantz CN. Pathogenesis of vertebral metastasis and epidural spinal cord compression. Cancer 1990;65:98–106.
2. Berry JL, Moran JM, Berg WS, Steffee AD. A morphometric study of human lumbar and selected thoracic vertebrae. Spine 1987;12:362–7.
3. Carter DR, Hayes WC. The compressive behavior of bones as a two phase porous structure. J Bone Joint Surg [Am] 1977; 59:954–62.
4. Constans JP, deDevitiis E, Donzelli R, Spaziante R, Meder JF, Haye C. Spinal metastases with neurologic manifestations review of 600 cases. J Neurosurg 1983;59:111–8.
5. DeWald RL, Bridwell KH, Prodromas C, Rodts MF. Reconstructive spinal surgery as palliation for metastatic malignancies of the spine. Spine 1985;10:21–6.
6. Haher TR, O'Brien M, Dryer JW, Nucci R, Zipnick R, Leone DJ. The role of the lumbar facet joints in spinal stability: Identification of alternate paths of loading. Spine 1994;19: 2667–71.
7. Holdsworth FW. Fractures, dislocations, and fracture-dislocations of the spine. J Bone Joint Surg [Am] 1970;52: 1534–1551.
8. Huiskes R, Hollister SJ. From structure to process, from organ to cell: Recent developments of FE-Analysis in orthopaedic biomechanics. J Biomech Eng 1993;115:520–7.
9. Keaveny TM, Hayes WC. A 20-year perspective on the mechanical properties of trabecular bone. J Biomech Eng 1993; 115:534–42.
10. Klisch SM, Duncan NA, Keaveny TM, Lotz JC. The relative effects of disc water content and bone modulus on vertebral body stresses. Presented at the International Society for Study of the Lumbar Spine, Burlington, Vermont, June 25–29, 1996.
11. Lotz JC, Cheal EJ, Hayes WC. Fracture prediction for the proximal femur using finite element models: Part I—linear analysis. J Biomech Eng 1991;113:353–60.
12. McAfee PC, Zdeblick TA. Tumors of the thoracic and lumbar spine: Surgical treatment via the anterior approach. J Spinal Disord 1989;2:145–54.
13. McBroom RJ, Hayes WC, Edward WT, Goldberg RP, White AA. Prediction of vertebral body compressive fracture using quantitative computed tomography. J Bone Joint Surg [Am] 1985;67:1206–14.
14. McGowan DP, Hipp JA, Takeuchi T, White AA III, Hayes WC. Strength reductions from trabecular destruction within thoracic vertebrae. J Spinal Disord 1993;6:130–6.
15. Mizrahi J, Silva MJ, Hayes WC. Finite element stress analysis of simulated metastatic lesions in the lumbar vertebral body. J Biomed Eng 1992;6:467–475.
16. Moran JM, Berg WS, Berry JL, Geiger JM, Steffee AD. Transpedicular screw fixation. J Orthop Res 1989;7:107–14.
17. Mosekilde L, Mosekilde L, Danielson CC. Biomechanical competence of vertebral trabecular bone in relation to ash density and age in normal individuals. Bone 1987;8:79–85.
18. Mosekilde L. Age related loss of vertebral trabecular bone mass and structure—biomechanical consequences. In: Mow VC, Ratcliffe A, Woo SL-Y, ed. Biomechanics of Diarthroidial Joints. Vol II. New York: Springer–Verlag, 1990:83–96.
19. Perrin RG. Symptomatic spinal metastases. Am Fam Physician 1989;39:165–71.
20. Phillips S, Fox N, Jacobs J, Wright WE. The direct medical costs of osteoporosis for American women aged 45 and older, 1986. Bone 1988;9:271–9.
21. Schultz A, Andersson G, Ortengren R, Haderspeck K, Nachemson A. Loads on the lumbar spine—validation of a biomechanical analysis by measurement of intradiscal pressures and myoelectic signals. J Bone Joint Surg [A] 1982;64: 713–20
22. Shirado O, Kaneda K, Tadano S, Ishikawa H, McAfee PC, Warden KE. Influence of disc degeneration on mechanism of thoracolumbar burst fractures. Spine 1992;17:286–92.
23. Silva MJ, Hipp JA, McGowan DP, Takeuchi T, Hayes WC. Strength reductions of thoracic vertebrae in the presence of transcortical osseus defects: Effects of defect location, pedicle disruption, and defect size. Eur Spine J 1993;2:118–25.

24. Silva MJ, Keaveny TM, Hayes WC. Load sharing between the shell and centrum in the lumbar vertebral body. Spine 1997; 22:140–50.
25. Suwito W, Keller T, Basu P, Weisberger A, Strauss A, Spengler D. Geometric and material property study of the human lumbar spine using the finite element method. J Spinal Disord 1992;5:50–9.
26. Tran NT, Watson NA, Tencer AF, Ching RP, Anderson PA. Mechanism of the burst fracture in the thoracolumbar spine: The effect of loading rate. Spine 1995;20:1984–8.

Address reprint requests to

Jeffrey C. Lotz, PhD
Orthopaedic Bioengineering Laboratory
Department of Orthopaedic Surgery
University of California San Francisco
533 Parnassus Avenue, Suite U-453
San Francisco, CA 94143-0514

THE EFFECT OF TUMOR SIZE, MATERIAL PROPERTIES AND LOADING RATE ON THE COMPRESSIVE RESPONSE OF METASTATICALLY INVOLVED VERTEBRAL BODIES.

Whyne CM, Hu SS, Lotz JC. Orthopaedic Bioengineering Laboratory, Department of Orthopaedic Surgery, University of California at San Francisco. UC Berkeley / UC San Francisco Graduate Group in Bioengineering.

Introduction: The vertebral column is the most frequent site of metastatic involvement of the skeleton, with up to 1/3 of all cancer patients developing metastases in the spinal column. Posterior vertebral body (burst) fracture can occur due to high impact loading or normal loading in metastatically compromised bones, resulting in significant clinical consequences including paralysis. While current medical imaging techniques are able to provide information on tumor size, location and progression, no objective criteria exists by which these data may be used to estimate risk of fracture and neurologic compromise. Further, the mechanism of collapse of the metastatically involved spine and correlations between the extent of tumor involvement and vertebral body collapse have not been fully understood. The objective of our study is to use a two-dimensional poroelastic axisymmetric finite element model to determine the effects of tumor size, material properties and loading rate in the assessment of burst fracture risk in metastatically involved vertebral bodies.

Methods: We developed a two-dimensional poroelastic axisymmetric finite element model of a spinal motion segment consisting of the first lumbar vertebral body and adjacent intervertebral disc. A finite element mesh consisting of 493 elements (8-noded quads and rebars) was generated and analyzed using commercial software (PATRAN 5.0, ABAQUS 5.6). The model was constructed to allow the inclusion of a centrally located tumor in the vertebral body, representing a 25% or 50% defect of the trabecular bone by volume. The vertebral body was composed of a cortical shell and endplate modeled isotropically and a transversely isotropic trabecular bone centrum, with properties chosen to represent a healthy young spine. The intervertebral disc consisted of cartilaginous endplate, nucleus pulposus and annulus fibrosus. The tumor tissue was modeled as a poroelastic isotropic material with the aggregate modulus and hydraulic permeability varied to represent a spectrum of material properties found in lytic lesions (H_A = 0.01 to 0.25 MPa, k = 5.0E-6 to 5.0E-5 m/s). The model was loaded axially under a uniform pressure of 1 MPa applied though the midplane of the intervertebral disc. Physiologic loading rates of 10 MPa/s and 100MPa/s were used. Focusing on the trabecular bone, our outcome variables were: displacement (to assess spinal canal encroachment and risk of endplate fracture), strain (indicating trabecular bone failure), and pore pressure (to determine the amount of load carried by the fluid phase).

Results: Tumor size had the greatest effect on vertebral body displacement, strain and pore pressure. Increasing tumor size from 25 to 50% yielded a 40% increase in maximum radial displacement, a 40% increase in tensile hoop and radial strains located at the axis of symmetry along the bone tumor interface, and a 130% increase in the compressive strain under the center of the endplate. Maximum trabecular bone displacement in the radial direction shifted from an area adjacent to the outer endplate in the intact vertebral body to the transverse midline when a defect was incorporated. Pore pressure in the trabecular bone increased by 160% and 280% respectively with the inclusion of 25% and 50% tumors into the vertebral body model as compared to the no tumor case. With a 10 fold reduction in loading rate, maximum endplate displacement and axial compressive strains were increased by 5 to 13% in the pathologic models. At the same time, maximum pore pressures in the vertebral body were reduced by 8% and were accompanied by a smaller overall pore pressure gradient and a slight (3%) reduction in radial displacement of the transverse midline. A 10 fold increase in tumor tissue permeability was found to have no effect on the results. However, a 25 fold increase in tumor aggregate modulus in the 50% defect model did result in small reductions in vertebral body strain (2 to 6%), displacement (0.5 to 3%) and pore pressure (2%).

Discussion: Increased tumor size was found to cause the greatest increase in vertebral body displacements, strains and pore pressure. As the size of defect increases, the location of maximum displacement and pore pressures would suggest a greater risk for endplate and radial vertebral body failure, indicating an increased likelihood of vertebral burst fracture. In contrast, the location of maximum strains in the healthy vertebral body indicates a higher likelihood of a compression fracture pattern rather than endplate or radial fracture. Greater maximum radial displacement values found at the transverse midline of the metastatically involved vertebral bodies may potentially correspond to bone encroachment into the spinal canal in a three-dimensional model. Loading rate was found to have the second strongest effect on vertebral body behavior. As loading rate was reduced, less load was carried by the fluid phase accounting for the lower pore pressures and radial displacement of the transverse midline and higher axial compressive strain in the trabecular bone. Variation of tumor tissue material properties did not have a large effect on the behavior of the trabecular bone centrum of the vertebral body, thus the primary site of the lytic tumor may not be significant in assessing failure risk.

This study uses a two-dimensional poroelastic axisymmetric finite element model to determine important parameters in burst fracture risk of metastatically involved vertebral bodies. Due to such an idealized model the results found here are used solely to make comparisons between the different cases (tumor size, loading rate, tumor tissue material properties). Future work is necessary to identify and incorporate other potentially important parameters such as variations in the trabecular bone quality, disc properties and tumor location. These simple models will form a basis for future work in three-dimensional modeling and experimental validation in attempts to understand the mechanism of burst fracture in metastatically involved vertebral bodies and ultimately determine better criteria to assess burst fracture risk in patients with spinal metastases.

VERTEBRAL BODY MODELING: THE EFFECTS OF POROELASTICITY AND LOADING RATE

*Whyne CM, Hu SS, +Lotz JC. *+Orthopaedic Bioengineering Laboratory, Department of Orthopaedic Surgery, University of California at San Francisco, San Francisco CA 94143-0514. Tel: (415) 476-7881, Fax:(415) 476-1128, Email: jlotz@itsa.ucsf.edu. *+UC Berkeley/UC San Francisco Graduate Group in Bioengineering.

Relevance to Musculoskeletal Conditions: In this study we question the importance of utilizing poroelasticity and the effect of loading rate in the modeling of spinal motion segments. This has significance in the study of both normal and pathologic spinal mechanics.

Introduction: The incidence of vertebral body fracture in the United States is estimated to be over 500,000 per annum. While the majority of vertebral body fractures do occur anteriorly, burst fracture patterns may arise from high impact loading or normal loading in bones compromised by neoplasm. Reports based on clinical observations have hypothesized that axial burst fractures occur due to internal pressurization and resultant explosion of the vertebral body following the endplate fracture. The objective of our study was to use a two-dimensional axisymmetric finite element model to assess the utility of poroelastic modeling techniques for analyzing spinal motion segments and effect of loading rate on the likelihood and location of vertebral body failure.

Methods: We developed a two-dimensional axisymmetric finite element model of a spinal motion segment consisting of the first lumbar vertebral body and adjacent intervertebral disc. A finite element mesh consisting of 493 elements (8-noded quads and rebars) was generated and analyzed using commercial software (PATRAN 5.0, ABAQUS 5.6). The vertebral body was loaded axially under a uniform pressure of 1 MPa applied though the intervertebral disc, which corresponds to an applied load of 1200N. The vertebral body was composed of a cortical shell and endplate modeled isotropically and a transversely isotropic trabecular bone centrum with properties chosen to represent a young healthy spine. The intervertebral disc consisted of cartilaginous endplate, nucleus pulposus and annulus fibrosus. The model was analyzed under a fully elastic configuration (both disc and vertebral body represented with elastic material properties), with a poroelastic disc and a linear elastic vertebral body (with and without restricted flow through the cartilaginous endplate), and as a fully poroelastic model. In the mixed elastic/poroelastic runs a physiologic loading rate level of 100MPa/s was applied. The poroelastic model was analyzed under a range of loading rates from 10,000 MPa/s (impact) to 4 MPa/s (slow walking). Our outcome variables were: radial displacement of the vertebral body midline (U1) as an indicator for spinal canal encroachment, endplate deformation (U2) as a measure of endplate fracture, and pore pressure (POR) to determine load carried by the fluid phase.

Results: Displacement and strain results in the elastically modeled vertebral body were found to be dependent on the disc representation used (elastic vs. poroelastic). Free or no flow through the endplate in the mixed models did not result in significant differences in vertebral body response *(Tbl 1)*.

Discussion: The boundary conditions applied to the vertebral body endplate are dependent on the constitutive assumptions of the intervertebral disc, and as such, effects the strain and displacement results in the trabecular bone centrum. Greater disc deformation in the axial and radial directions in the fully elastic model create different loading conditions applied to the cortical endplate of the vertebral body, and thus different responses within the vertebral body itself. For analyses aimed at studying the responses of the intervertebral disc alone, our results suggest it is reasonable to utilize a mixed model. The fully poroelastic results in the intervertebral disc are bounded by the results derived from the mixed models (with a free flow boundary at the endplate simulating a fully poroelastic model at a slow loading rate and a no flow boundary condition simulating fast loading). However, results for strains and displacements in the poroelastic vertebral body are not bounded by the mixed model results. The fully poroelastic representation yields higher maximum principle tensile strains and radial displacement in the vertebral body than found in the mixed models and lower maximum principle compressive strains and axial displacement. The inclusion of the fluid phase into the vertebral body results in a portion of the spinal load being supported by the liquid, reducing the solid strains in the axial direction in the trabecular bone. At the same time, the incompressibility of the fluid phase will cause expansion and higher strains to develop in the radial direction within the vertebral body. As the loading rate is increased, higher values of compressive strains and lower values of tensile strains were predicted in the vertebral body. Simultaneously, maximum pore pressures within the nucleus were found to increase, while pore pressures in the vertebral body decrease. This opposing trend was due to the diffusion time constant of the nucleus being on the order of 10^5 s whereas the diffusion time constant for the trabecular bone is on the order of 10^{-1}s. As fluid does not have time to escape from the nucleus under higher loading rates, the incompressibility of the fluid phase in the nucleus causes increased axial deformation of the vertebral body endplate. These results indicate an increased likelihood for endplate failure in vertebral bodies loaded at higher rates, potentially leading to burst fracture patterns if the endplate fracture permits the nucleus to enter and pressurize the vertebral body. While this study is limited by the use of a two-dimensional axisymmetric model, results of this simplified analysis provide justification for the use of more complex three-dimensional poroelastic models and show the importance of loading rate. Although the cost of poroelastic modeling is relatively large, both in terms of determination of additional poroelastic material properties and extended CPU time (especially for three-dimensional models), a purely elastic approach may not be sufficient to reproduce the complex behavior exhibited by this two phase structure.

	Rate(MPa/s)	U1 mm	U2 mm	POR(MPa)
Elastic	-	0.049	-0.048	-
Mixed (no flow)	100	0.050	-0.072	-
Mixed (free flow)	100	0.048	-0.073	-
Poroelastic	100	0.056	-0.067	0.33
Poroelastic	10	0.067	-0.063	0.50

Table 1: Maximum values from the vertebral body centrum.

Acknowledgments: Funding for this work was provided by UC San Francisco REAC, NSERC (Canada) and USAMRC.

☐ One or more of the authors have received something of value from a commercial or other party related directly or indirectly to the subject of my presentation.

☒ The authors have not received anything of value from a commercial or other party related directly or indirectly to the subject of my presentation.

POROELASTIC FINITE ELEMENT MODELING OF METASTATICALLY INVOLVED VERTEBRAL BODIES

*Whyne CM, Hu SS, +Lotz JC. Orthopaedic Bioengineering Laboratory, Department of Orthopaedic Surgery, University of California at San Francisco, San Francisco CA 94143-0514. Tel: (415) 476-7881, Fax:(415) 476-1128, Email: jlotz@itsa.ucsf.edu. UC Berkeley/UC San Francisco Graduate Group in Bioengineering.

Relevance to Musculoskeletal Conditions: In this study we attempt to identify important parameters necessary for the assessment of burst fracture risk in metastatically involved vertebral bodies.

Introduction: The vertebral column is the most frequent site of metastatic involvement of the skeleton, with up to 1/3 of all cancer patients developing metastases in the spine. Posterior vertebral body (burst) fracture can occur due to high impact loading or normal loading in metastatically compromised bones, resulting in significant clinical consequences including paralysis. Strength prediction for metastatically involved vertebral bodies can be used to estimate the risk of vertebral body failure, including fracture location and the potential for spinal canal encroachment. To date, the mechanism of collapse of the metastatically involved spine and its dependence on the extent of tumor involvement have not been fully understood. The objective of our study was to use a two-dimensional poroelastic axisymmetric finite element model to determine the effects of tumor size, material properties and loading rate in the assessment of burst fracture risk in metastatically involved vertebral bodies.

Methods: We developed a two-dimensional poroelastic axisymmetric finite element model of a spinal motion segment consisting of the first lumbar vertebral body and adjacent intervertebral disc. A finite element mesh consisting of 493 elements (8-noded quads and rebars) was generated and analyzed using commercial software (PATRAN 5.0, ABAQUS 5.6). The model was constructed to allow the inclusion of a centrally located tumor in the vertebral body, representing a 25% or 50% defect of the trabecular bone by volume. The vertebral body was composed of a cortical shell and endplate modeled isotropically and a transversely isotropic trabecular bone centrum, with properties chosen to represent a healthy young spine. The intervertebral disc consisted of cartilaginous endplate, nucleus pulposus and annulus fibrosus. The tumor tissue was modeled as a poroelastic isotropic material with the aggregate modulus and hydraulic permeability varied to represent a spectrum of material properties found in lytic lesions (H_A = 0.01 to 0.25 MPa, k = 0.0005 to 0.005 m/s). The model was loaded axially under a uniform pressure of 1 MPa applied though the midplane of the intervertebral disc. Physiologic loading rates of 10 MPa/s and 100MPa/s were used. Focusing on the trabecular bone, our outcome variables were: displacement (to assess spinal canal encroachment and risk of endplate fracture), strain (indicating trabecular bone failure), and pore pressure (to determine the amount of load carried by the fluid phase).

Results: Tumor size had the greatest effect on vertebral body displacement, strain and pore pressure. Increasing tumor size from 25 to 50% yielded a 40% increase in maximum radial displacement, a 40% increase in tensile hoop and radial strains located at the axis of symmetry along the bone tumor interface, and a 130% increase in the compressive strain under the center of the endplate. Maximum trabecular bone displacement in the radial direction shifted from an area adjacent to the outer endplate in the intact vertebral body to the transverse midline when a defect was incorporated. Pore pressure in the vertebral body trabecular bone also increased by 160% and 280% respectively with the inclusion of 25% and 50% tumors into the vertebral body model as compared to the no tumor case. With a 10 fold reduction in loading rate, maximum endplate displacement and axial compressive strains were increased by 5 to 13% in the pathologic models. At the same time, maximum pore pressures in the vertebral body were reduced by 8% and were accompanied by a smaller overall pore pressure gradient. A 10 fold increase in tumor tissue permeability was found to have no effect on the results. However, a 25 fold increase in tumor aggregate modulus in the 50% defect model resulted in small reductions in vertebral body strain (2 to 6%), displacement (0.5 to 3%) and pore pressure (2%).

Discussion: Increased tumor size was found to cause the greatest increase in vertebral body displacements, strains and pore pressure. The location of maximum displacement and pore pressures suggest a greater risk for endplate and radial vertebral body failure (i.e. an increased likelihood of vertebral burst fracture) as the size of defect increases. Greater maximum radial displacement values predicted at the transverse midline of the vertebral body may potentially correspond to encroachment into the spinal canal in a three-dimensional model. Loading rate was found to have the second strongest effect on vertebral body behavior. As loading rate was reduced, less load was carried by the fluid phase accounting for the lower pore pressures and higher axial compressive strains and displacements in the trabecular bone. Variation of tumor tissue material properties did not have a large effect on the behavior of the trabecular bone centrum of the vertebral body, thus the primary site of the lytic tumor may not be significant in assessing failure risk. This study uses a two-dimensional poroelastic axisymmetric finite element model to determine important parameters in burst fracture risk of metastatically involved vertebral bodies. Due to such an idealized model the results found here are used solely to make comparisons between the different cases (tumor size, loading rate, tumor tissue material properties). Additional work is necessary to identify and incorporate other potentially important parameters such as variations in the trabecular bone quality, disc properties and tumor location. These simple models will form a basis for future work in three-dimensional modeling and experimental validation with the goal of determining better criteria to assess burst fracture risk in patients with spinal metastases.

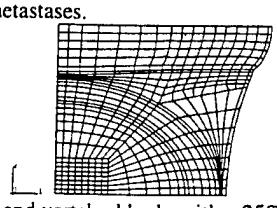

Figure 1: Loaded disc and vertebral body with a 25% tumor.

Acknowledgments: Funding for this work was provided by UC San Francisco REAC, NSERC (Canada) and USAMRC.

☐ One or more of the authors have received something of value from a commercial or other party related directly or indirectly to the subject of my presentation.

☒ The authors have not received anything of value from a commercial or other party related directly or indirectly to the subject of my presentation.

Lotz, Jeffrey (1)
533 Parnassus Avenue/San Francisco,
CA/94143-0514
415 476 7881 / Fax: 415 476 1128 /
jlotz@itsa.ucsf.edu

Preferences and Keywords

Tumors;Metastases;Biomechanical Properties;Mechanical Testing

Disclosure

ABSTRACT NO. _____
PAPER NO. _____

MECHANICAL PROPERTIES OF METASTATIC TUMORS IN BONE

*Whyne, C; *Hu, S; +*Lotz, J
+-*Orthopaedic Bioengineering Laboratory, Department of Orthopaedic Surgery, University of California, San Francisco, San Francisco, CA. 533 Parnassus Avenue/San Francisco, CA/94143-0514, 415 476 7881, Fax: 415 476 1128, jlotz@itsa.ucsf.edu

Introduction: Breast, prostate, lung and renal cancers are the most common primary tumors which metastasize to bone. In order to model and understand the fracture mechanism in the metastatically involved skeleton, one needs to prescribe the mechanical properties of the tumor tissue. Unfortunately, little quantitative data exists for this purpose. Previous models examining lytic tumor behaviour have utilized properties of other soft tissues (ie brain tissue) or have modeled such lesions as voids. The objective of our study was to measure the biphasic material properties of human lytic tumor tissue which has metastasized to bone, and to determine if these mechanical properties are dependent on tumor type and/or composition.

Methods: Lytic tumor tissue specimens were harvested from human bone and tested under a confined compression uniaxial creep protocol. Tissue specimens were fresh frozen, cut and punched directly into a titanium confining chamber resulting in a cylindrical plug 1-2mm in height by 5 mm in diameter. Each specimen was sandwiched between a porous glass platen (below) and a low friction acrylic platen (above). A constant load was applied to the specimen inside the confining chamber and a linear variable differential transformer was used to measure the change in displacement over time. The experiments were conducted in a saline bath at 37 degrees Celsius. Each experiment was run until equilibrium had been reached. Applied loads ranged from 0.5 g to 1.5 g. Initial apparatus testing was done using a hydrogel material to ensure the precision and repeatability of the experimental protocol.

Specimens from 14 lytic tumors which had metastasized to bone were harvested. These include specimens from breast, lung, renal, multiple myeloma and other cancers. Multiple specimens were tested for each tumor (with 3 exceptions due to small tumor size) to determine the intra-specimen variability due to both the testing protocol and inhomogeneities within the tumor. This resulted in a total of 27 specimens which underwent mechanical testing.

The mechanical behaviour of the tumor tissue was modeled using linear biphasic theory. This approach assumes that the solid phase of the tissue is isotropic, homogeneous and linearly elastic and that the fluid is inviscid and incompressible. The outcome variables for each specimen were the aggregate compressive modulus (H_A) and the hydraulic permeability (k). To determine these linear biphasic material properties of the tumor tissue specimens, the displacement vs time data was curve fit using a numerical minimization of least squares technique (Matlab 5.0) to the solution for creep displacement u(t) predicted by this model:

$$\frac{u(t)}{h} = \frac{P}{H_A}\left\{1 - 8\sum_{n=0}^{9}\frac{\exp(-tH_A k(\pi(1+2n)/2h)^2}{(\pi(1+2n))^2}\right\}$$

where Pa is the applied stress in MPa, h is the initial specimen thickness in mm, and t is time in seconds. Applied loads were adjusted so as to meet the small strain behaviour assumed in this theory.

Following testing, the histology of each tumor specimen was analyzed. The specimens were immersed in formalin and run through an H & E stain. Visual inspection of the slides was used to determine the cellular vs. stromal content of the tissue present in each specimen. The cellularity data was organized into four groups: 0-25% cells, 25-50% cells, 50-75% cells, and 75-100% cells

Standard analysis of variance procedures were performed to compare specimen group means and to estimate the effect of the specimen variables (tumor type and cellularity) on the measured parameters of interest (H_A and k). A Fischer LSP test was used to determine differences between groups where appropriate.

Results: The aggregate modulus (H_A) of the tumor tissue tested yielded a mean of 0.0034 MPa with a standard deviation of 0.0016 MPa. The mean hydraulic permeability (k) of the specimens was 0.61 mm^4/Ns with a standard deviation of 0.44 mm^4/Ns.

Tumors with a higher percentage of stromal content were found to be stiffer than those with a more cellular composition. The aggregate modulus of specimens with less than 50% cellularity was 76 percent more than that from more cellular tumors (0.0051 MPa vs 0.0029 MPa , $p<0.05$). As well, tumors with lower cellularity were found to have a higher hydraulic permeability, although this result did not reach the level of statistical significance (<25% cellularity, k=1.13 mm^4/Ns; >25% cellularity, k=0.54 mm^4/Ns, p=0.066). No significant differences in aggregate modulus or hydraulic permeability were found between tumors of different types.

Discussion: Tumor tissue specimens with a higher stromal content were found to behave stiffer than more cellular specimens. A higher percentage of stromal matrix increases the interconnectivity of the tumor tissue yielding both a higher compressive aggregate modulus and lower hydraulic permeability than more cellular specimens. No significant differences in mechanical properties were found between different tumor types. This finding is not surprising considering the histological variation seen between tumors of the same type and even within different areas of individual specimens.

The values of H_A and k reported here are consistent with those measured for other hydrated tissues. For comparison, results from experimentation done on annulus fibrosus and cartilage have yielded much stiffer and less permeable results (annulus: H_A=0.12 MPa, k=0.013 mm^4/Ns; cartilage: H_A=0.3 to 1.5 MPa, k=0.01to 0.001 mm^4/Ns). The high fluid content of the tumors and the poor interconnectivity of the solid matrix would support the low aggregate modulus and high permeability values measured for this tissue.

In order to adequately model the behaviour of the metastatically involved skeleton using theoretical or finite element analysis techniques, it is necessary to know the biphasic material properties of the tumor tissue itself. Previous models developed to study burst fracture in the metastatically involved spine have neglected the material properties of such lesions. Bony defects have been modeled as voids, neglecting any effects from the mass and fluid behavior of tumor material. Due to these misrepresentations, the risk of burst fracture and neurologic injury in these studies may have been underestimated. Determination of tumor tissue material properties will enable the development of more accurate models of the metastatically involved spine which may be better able to simulate the pattern of burst fracture and clarify the risk of neurologic compromise.

Determination of the biphasic material properties of lytic lesions also has importance in developing effective tumor-drug transport models. In order for therapeutic agents to reach cancer cells, these large macromolecules must travel from the vessels across the interstitial matrix of the tumor. Higher permeabilities found in more cellular tumors may facilitate the transport of therapeutic agents to these metastases in comparison to tumors with higher stromal contents. Heterogeneous neoplasms, which incorporate areas of high cellularity and regions consisting mainly of stromal matrix may require sophisticated modeling to accurately gauge drug delivery throughout the tumor.

This study provides values for the mechanical properties of lytic bone metastases. Understanding the mechanical behaviour of this tissue may help to better focus future treatment of lytic bony metastases through improved drug delivery and better assessment of fracture risk.

Acknowledgements: Funding for this research was provided by NSERC (Canada) and USAMRC.

Lotz, Jeffrey (1)
533 Parnassus Avenue/San Francisco,
CA/94143-0514
415 476 7881 / Fax: 415 476 1128 /
jlotz@itsa.ucsf.edu

Preferences and Keywords

Tumors;Metastases;Mechanical Testing;Finite Element Analysis;Bone Mineral Density

Disclosure

ABSTRACT NO. _____
PAPER NO. _____

THE EFFECT OF BONE DENSITY ON THE METASTATICALLY INVOLVED SPINE: THREE-DIMENSIONAL FINITE ELEMENT MODELING AND EXPERIMENTAL VALIDATION

*Whyne, C; *Hu, S; +*Lotz, J

+*Orthopaedic Bioengineering Laboratory, Department of Orthopaedic Surgery, University of California, San Francisco, San Francisco, CA. 533 Parnassus Avenue/San Francisco, CA/94143-0514, 415 476 7881, Fax: 415 476 1128, jlotz@itsa.ucsf.edu

Introduction: The vertebral column is the most frequent site of metastatic involvement of the skeleton, with up to 1/3 of all cancer patients developing tumors in the spine. Posterior vertebral body (burst) fractures can occur under normal loading conditions in the metastatically involved spine resulting in significant neurologic consequences. The objectives of this study were to develop and experimentally validate a three-dimensional finite element model which can adequately predict the behaviour of metastatically involved spinal motion segments and to determine the effect of reduced bone density on the risk of neurologic injury.

Methods: Fresh-frozen spinal motion segments were harvested from 6 cadaveric spines through the midplane of the 12th thoracic and 2nd lumbar vertebrae. Bone mineral densities were determined for all specimens using DEXA in the lateral projection. The spinal motion segments were tested in axial compression using a servo-hydraulic MTS machine. Specimens were put under a -100 N preload followed by a load of -800 N which was applied to the specimen at a rate of 16000 N/s. This load approximates the compressive force on the lumbar spine for an individual standing upright, holding a 3.8 kg mass with outstretched arms.

Following testing of the intact specimen a defect was introduced into the trabecular centrum of L1 (Figure 1). A 16 mm diameter hole was cored into the trabecular centrum through the lateral wall, without breaking through the opposing cortex. The core was removed from the centrum and the defect filled with a 0.5% solution of agarose gel. This gel was formulated to mimic the average material properties of lytic tumor in bone. The core was dissected to yield an end-cap of trabecular bone and cortical shell which was reattached to the vertebral body using PMMA, filling all gaps for a tight seal. The defects occupied approximately 15% of the trabecular bone centrum by volume. Biomechanical testing of the specimens containing these defects was repeated as described above.

We developed a three dimensional poroelastic finite element model of the first lumbar vertebra and adjacent intervertebral discs, symmetric about the sagittal plane and incorporating anatomical vertebral body curvature based on average values reported for L1 (Figure 1). The posterior arch was included in the model, although no other posterior elements were modeled. The model was designed to include a centrally located hemi-elliptical tumor occupying 15%, 30% or 45% of the trabecular bone centrum by volume. The mesh consisted of 5668 elements (20-noded bricks) and was generated and analyzed using commercial software (PATRAN 7.0; ABAQUS 5.7).

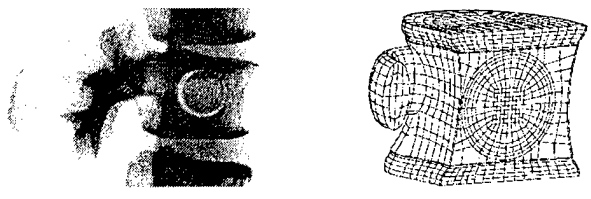

Figure 1: Xray of a Spinal Motion Segment with an Artificially Introduced Defect and the Metastatically Involved Vertebral Body Finite Element Model.

In order to validate the model, analyses were conducted under conditions similar to the experimental testing. The model was loaded in axial compression through the midplane of the superior intervertebral disc with a pressure of -0.62 MPa (corresponding to an -800 N load), at a loading rate of 16000 N/s in accordance with the experimental protocol.

Our goal was to assess the effects of bone mineral density on the potential for neurologic compromise in the metastatically involved spine. To address this goal and compare our model and experimental results, we determined the load induced spinal canal narrowing (LICN) and the hoop strain at the midline of the anterior vertebral body wall.

Results: The experimental results demonstrated an increase in LICN from 64% to 400% (232±107%) when a 15% tumor was included as compared to the intact specimens. This percentage change in LICN was found to increase as bone mineral density decreased (Figure 2). Tensile hoop strains along the midline of the anterior wall also increased with the inclusion of a tumor from 146% to 1067% (518±338%). This percentage change in tensile hoop strain similarly increased with decreasing bone mineral density.

In comparing the intact and 15% tumor finite element models, our poroelastic finite element model predicted a 104% increase in LICN with the inclusion of the tumor as compared to the intact model with a trabecular bone apparent density of 0.10 g/cm^3. When the trabecular bone apparent density was increased to 0.17 g/cm^3 the model predicted an 83% increase in LICN. In comparing bone density to canal narrowing, similar to the experimental results, lower bone density values predicted higher percentage increases in canal narrowing with the inclusion of the vertebral defect.

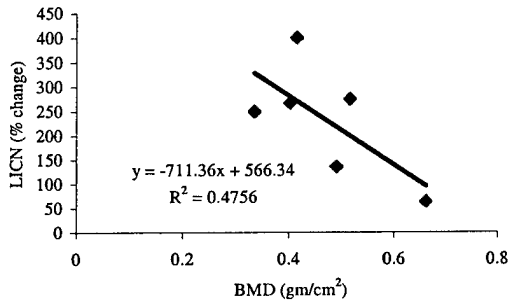

Figure 2: Bone Mineral Density vs. % Change in Canal Narrowing between the Intact and Metastatically Involved Vertebral Bodies – Experimental data.

A 70% increase in the apparent density of the trabecular bone, caused a 157% reduction in LICN and a 63% reduction in the tensile hoop strain in the 15% tumor model. Similarly, in the experimental testing of the metastatically involved specimens, a 70% increase in bone mineral density yielded a reduction of 163% in LICN and a decrease of 217% in tensile hoop strain.

Discussion: Inclusion of a metastatic defect into the vertebral body increases both narrowing of the spinal canal and tensile hoop strains at the vertebral midline. Our idealized model serves as a good predictor of both changes in canal narrowing and tensile hoop strains as compared to our experimental data.

Decreasing vertebral bone density was found to increase the narrowing of the spinal canal and tensile hoop strains at the vertebral body midline. Failure of the vertebra due to elevated tensile hoop strains would correspond to clinical patterns seen in the burst fracture of metastatically involved vertebral bodies in which pieces of bone and tumor tissue may be retropulsed into the spinal canal. Such increases in tensile hoop strains and canal narrowing have important implications for an increased risk of neurologic compromise in patients with reduced vertebral bone densities. Clinically, our data suggest that bone mineral density may be one important predictor of burst fracture risk and neurologic injury in patients with vertebral metastases.

In this study we have developed and validated a three-dimensional finite element model of a metastatically involved spinal motion segment. Future use of this idealized model and our experimental data will allow us to examine the effects of increased loads and loading rates, tumor size, pedicle involvement and disc quality in examining burst fracture risk in the metastatically involved spine.

Acknowledgements: Funding for this research was provided by NSERC (Canada) and USAMRC.